

DEVELOPMENT OF UAV-BASED PAVEMENT CRACK IDENTIFICATION
SYSTEM USING ARTIFICIAL INTELLIGENCE

A THESIS SUBMITTED TO
THE GRADUATE SCHOOL OF NATURAL AND APPLIED SCIENCES
OF
THE MIDDLE EAST TECHNICAL UNIVERSITY

BY

AHMET BAHADDİN ERSÖZ

IN PARTIAL FULFILLMENT OF THE REQUIREMENTS
FOR
THE DEGREE OF MASTER OF SCIENCE
IN
CIVIL ENGINEERING

SEPTEMBER 2016

Approval of the thesis:

**DEVELOPMENT OF UAV-BASED PAVEMENT CRACK
IDENTIFICATION SYSTEM USING ARTIFICIAL INTELLIGENCE**

submitted by **AHMET BAHADDİN ERSÖZ** in partial fulfillment of the requirements for the degree of **Master of Science in Civil Engineering Department, Middle East Technical University** by,

Prof. Dr. Gülbın Dural Ünver _____
Dean, Graduate School of **Natural and Applied Sciences**

Prof. Dr. İsmail Özgür Yaman _____
Head of Department, **Civil Engineering**

Asst. Prof. Dr. Onur Pekcan _____
Supervisor, **Civil Engineering Dept., METU**

Examining Committee Members:

Prof. Dr. Erdal Çokça _____
Civil Engineering Dept., METU

Asst. Prof. Dr. Onur Pekcan _____
Civil Engineering Dept., METU

Prof. Dr. Ahmet Türer _____
Civil Engineering Dept., METU

Asst. Prof. Dr. Hande Işık Öztürk _____
Civil Engineering Dept., METU

Asst. Prof. Dr. Selen Pehlivan _____
Computer Engineering Dept., TED University

Date: 06.09.2016

I hereby declare that all information in this document has been obtained and presented in accordance with academic rules and ethical conduct. I also declare that, as required by these rules and conduct, I have fully cited and referenced all material and results that are not original to this work.

Name, Last name: Ahmet Bahaddin Ersöz

Signature : 

ABSTRACT

DEVELOPMENT OF UAV-BASED PAVEMENT CRACK IDENTIFICATION SYSTEM USING ARTIFICIAL INTELLIGENCE

Ersöz, Ahmet Bahaddin

M.S., Department of Civil Engineering

Supervisor: Asst. Prof. Dr. Onur Pekcan

September 2016, 92 pages

Building an accurate, robust and timely working Pavement Crack Identification System (PCIS) is one of the challenging components of Pavement Management Systems (PMSs). The ultimate aim of PCIS is to have autonomous inspection methods integrated into PMS. This way a modern PCIS may replace the currently used methods to eliminate their shortcomings such as being labor intensive, biased and time consuming. With the recent introduction of Unmanned Aerial Vehicles (UAVs), engineering research studies are inclined towards their use in various applications. In this study, UAVs are employed to capture the images of the pavement surface, from which pavement cracks are detected using digital image processing techniques and classified with a machine learning algorithm called Support Vector Machines (SVMs). The proposed pavement crack identification method using images includes preliminary operations, making the images uniformly illuminated and noise free. Comparatively darker regions in pre-processed images called connected components are obtained using automated thresholding. Through geometric features extracted from

connected components, SVMs are used to classify the cracks, through which the connected components are classified into four groups: longitudinal cracks, transverse cracks, alligator cracks and non-crack regions. A case study was performed to measure the performance of the proposed method. The crack prediction results were quite successful. The proposed PCIS has a few benefits such as being cheap and computationally efficient and therefore, it can be used in practical pavement management applications successfully.

Keywords: Pavement Crack Identification, Support Vector Machines, Machine Learning, Unmanned Aerial Vehicles, Digital Image Processing

ÖZ

YAPAY ZEKA KULLANARAK İHA TABANLI YOL ÜSTYAPI ÇATLAĞI TANIMLAMA SİSTEMİ GELİŞTİRİLMESİ

Ersöz, Ahmet Bahaddin

Yüksek Lisans, İnşaat Mühendisliği Bölümü

Tez Yöneticisi: Yrd. Doç. Dr. Onur Pekcan

Eylül 2016, 92 sayfa

Doğru, güvenilir ve hızlı çalışan bir yol üstyapı çatlağı tanımlama sistemi oluşturmak, yol üstyapı yönetim sistemlerinin zorlu aşamalarından biridir. Yol üstyapı çatlağı tanımlama sistemlerinin nihai amacı; kullanımda olan yol üstyapı yönetim sistemlerinin bir parçası olarak otonom yöntemlere sahip olmaktır. Bu şekilde modern bir çatlak tanımlama sistemi, hala kullanımda olan sistemlerin; yoğun işgücü gerektirmesi, kişiye bağlı ve zaman alıcı olması gibi eksikliklerini gidermek için, var olan yöntemlerin yerine geçebilir. Son zamanlarda İnsansız Hava Araçlarının (İHA) yaygınlaşmasıyla, mühendislik araştırma çalışmaları İHA'ların çeşitli uygulamalarda kullanılması yönüne kaymıştır. Bu çalışmada, yol üstyapı yüzeyinden resimler almak için İHA'lar kullanılmış, yol üstyapı çatlakları dijital görüntü işleme teknikleri kullanılarak tespit edilmiş ve Destek Vektör Makinesi (DVM) olarak adlandırılan bir makine öğrenmesi algoritmasıyla da çatlaklar sınıflandırılmıştır. Önerilen yol üstyapı çatlağı tanımlama yöntemi resim gürültüsü ve yansımaya problemlerini ortadan kaldırır

bazı ön işlemler içerir. Ön işlem görmüş resimlerde otomatikleştirilmiş eşikleme yöntemi kullanılarak, bitişik parçalar olarak adlandırılan, nispeten daha koyu olan bölgeler elde edilir. Bitişik parçalardan çıkartılan geometrik özellikler vasıtasiyla DVM'ler, çatlakları boylamasına çatlak, enlemesine çatlak, timsah sırtı çatlığı ve çatlak olmayan bölge olmak üzere 4 farklı gruba ayırır. Önerilen yöntemin performansını ölçmek için bir arazi çalışması gerçekleştirilmiştir. Sonuçlar değerlendirildiğinde, çatlak tahminleri oldukça başarılıdır. Önerilen yol üstyapı çatlığı tanımlama sisteminin ucuz ve hesaplama açısından verimli olması gibi birtakım faydaları vardır. Dolayısıyla pratik yol üstyapı yönetim uygulamalarında başarıyla kullanılabilir.

Anahtar Kelimeler: Yol Üstyapı Çatlığı Tanımlama, Destek Vektör Makineleri, Makine Öğrenmesi, İnsansız Hava Araçları, Dijital Görüntü İşleme

Dedicated to my beloved family...

ACKNOWLEDGEMENTS

Foremost, I would like to express my deepest gratitude to my supervisor Dr. Onur Pekcan for his excellent guidance, caring, patience and enthusiasm throughout my research. He has continuously encouraged me since the first day that we met. He has always been available to help me, even at night times and holidays. Without his advice and encouragement, I would never have accomplished finishing this study.

I would also like to thank the examining committee members for accepting to be a jury member for my thesis defense and spending their valuable time for reviewing my thesis and providing feedback.

My special thanks goes to Türker Teke, who helped selflessly when I needed it most. I am greateful for his kind support, useful discussions and great friendship. I really enjoyed the happy days I spent with him.

I would like to express my thanks to colleagues Ali Gharibdoust, Murat Altun, Yılmaz Emre Sarıcıçek, Gizem Can, Makbule İlgaç, Berkan Söylemez, Yağızer Yalçınér, Emir Ahmet Oğuz, Muhammed Batuhan Tezcan, Burak Akbaş and others for their support in many instances during my thesis journey.

I am thankful to my friends İbrahim Yıldırın, Murat Tokar, Oğuzhan Evsen and Murat Beycan for always being there when I need courage and help for more than a decade.

I also would like to thank Republic of Turkey, Prime Ministry Disaster & Emergency Management Authority (AFAD) for providing the UAV equipment in the scope of CANKUŞ Project (No: UDAP-Ç-12-13).

Last but not least, I would like to thank my dear family. Without their support, patience and trust, I would never have completed this study. Therefore, this thesis is dedicated to them; especially remembering my mother Meryem Ersöz and my father Ayhan Ersöz for their endless love, understanding and tolerance.

TABLE OF CONTENTS

ABSTRACT	v
ÖZ	vii
ACKNOWLEDGEMENTS	x
TABLE OF CONTENTS	xi
LIST OF TABLES	xiii
LIST OF FIGURES	xiv
LIST OF ABBREVIATIONS	xvi
CHAPTERS	
1. INTRODUCTION	1
1.1. Overview and Problem Statement	1
1.2. Objectives of the Research	4
1.3. Scope of the Thesis.....	5
1.4. Thesis Organization.....	7
2. LITERATURE REVIEW.....	9
2.1. Data Collection Platforms	9
2.1.1. Manual Inspection Methods	10
2.1.2. Truck Based Systems	12
2.1.3. Unmanned Aerial Vehicles	17
2.2. Data Processing Techniques.....	24
3. PAVEMENT CRACK IDENTIFICATION METHOD	35
3.1. Crack Candidate Detection.....	36

3.1.1.	Non-uniform Background Illumination Correction	37
3.1.2.	Wavelet Denoising	40
3.1.3.	Local Thresholding based Image Segmentation	43
3.1.4.	Post Processing and Image Enhancement	45
3.1.4.1.	Median Filtering.....	45
3.1.4.2.	Noise Cancellation	47
3.1.4.3.	Morphological Closing Operation	48
3.2.	Crack Classification.....	54
3.2.1.	Feature Extraction	54
3.2.2.	Classification of Crack Types based on SVM	59
3.2.2.1.	SVM Theory	60
3.2.2.2.	Multi-Class SVM.....	67
4.	FIELD EXPERIMENTS	69
4.1.	Crack Candidate Detection.....	72
4.2.	Crack Classification.....	73
4.3.	Results and Discussion	77
5.	SUMMARY, CONCLUSIONS AND FUTURE WORK.....	83
5.1.	Summary.....	83
5.2.	Conclusions	85
5.3.	Future Work.....	87
	REFERENCES.....	89

LIST OF TABLES

TABLES

Table 1 - Typical Connected Component Feature Values	58
Table 2 - Specifications of DJI Inspire 1 Used in the Experiments	71
Table 3 - Representative Training Data Set	75
Table 4 - Number of Classified Connected Components.....	75
Table 5 - Statistical Measures	79

LIST OF FIGURES

FIGURES

Figure 1 - Schematic Representation of the Pavement Crack Identification System	6
Figure 2 - Manual Inspection Methods in the Field	10
Figure 3 - Automated Road Analyzer Vehicle	13
Figure 4 - Laser Crack Measurement System and Projection of Laser	16
Figure 5 - Visualization of 3D Pavement Surface Data	17
Figure 6 – Type of UAVs	19
Figure 7 - Process For Facade Modeling	21
Figure 8 - Proposed UAV-Based Remote Sensing System For Unpaved Road Condition Assessment	22
Figure 9 - Road Information Detected by this System	23
Figure 10 - System Architecture For Crack Detection and Classification	27
Figure 11 - 2D Feature Space Used For Crack Classification	29
Figure 12 - Joint and Bridged Defect Sample	30
Figure 13 - Flow Chart of the Proposed Cracktree Method	32
Figure 14 - Flow Chart of the Proposed Algorithm	36
Figure 15 - A Disk Shape Filter Where the Radius is 3 Pixels	38
Figure 16 – Non-uniform Background Illumination Correction	39
Figure 17 - Wavelet Denoising	42
Figure 18 – Thresholding	44
Figure 19 - An Example of Median Filtering	46
Figure 20 - Median Filtering	47
Figure 21 - Noise Removal	48
Figure 22 - Erosion of the Object Using 3 x 3 Structuring Element	50
Figure 23 - Dilation of the Object Using 3 x 3 Structuring Element	50
Figure 24 - Result of Applying Opening Operation	52
Figure 25 - Result of Applying Closing Operation	52

Figure 26 - Diamond Shape Structuring Element with 5 Pixels Radius	53
Figure 27 - Morphological Closing Operation Illustration	53
Figure 28 – Visualization of Geometric Features	58
Figure 29 - An Optimal Separating Hyperplane	60
Figure 30 - Non-Linear Mapping: The 2D Input Space is Projected on 3D Space ...	66
Figure 31 - Image Locations on Middle East Technical University Campus	70
Figure 32 - DJI Inspire 1 Quadcopter	71
Figure 33 - Results of Crack Candidate Detection Algorithm For Different Crack Categories.....	74
Figure 34 - Classification of Crack Types	76
Figure 35 - Actually Non-Crack Region Classified As Longitudinal Crack	78
Figure 36 - Broken Alligator Crack	78
Figure 37 - Multiple Crack Identification	80

LIST OF ABBREVIATIONS

DSLR	Digital Single-Lens Reflex
FOV	Field of View
FPS	Frames Per Second
GPS	Global Positioning System
IMU	Inertial Measurement Unit
LiPO	Lithium Polymer
LTPP	Long-Term Pavement Performance
METU	Middle East Technical University
NCHRP	National Cooperative Highway Research Program
PCIS	Pavement Crack Identification System
PMS	Pavement Management System
RBF	Radial Basis Function
SE	Structuring Element
SVM	Support Vector Machine
UAV	Unmanned Aerial Vehicle
UAVS	Unmanned Aerial Vehicle Systems

CHAPTER 1

INTRODUCTION

1.1. Overview and Problem Statement

Roads are ones of essences of human life, playing a significant role through reducing the distance among people, markets, services and knowledge. They are the most basic tools for adjusting the balance between supply and demand in terms of the infrastructure. The economic development and total length of paved roads of a country highly depends on each other, since the most widely used mode of transportation system is still the road transportation in the world. Like any other civil engineering structure, road pavements need to be strong and durable under various loading conditions and environment throughout their lifetime. With this purpose in mind, they must be designed, constructed and maintained properly.

Among the design, construction and maintenance stages of road construction, the rehabilitation of pavements keeps a special place considering that it is inevitable during the lifetime of pavements after they are constructed. Every year, transportation agencies allocate enormous amount of budget for pavement rehabilitation and maintenance activities of existing pavements. As mentioned in USA's Fiscal Year 2016 report, USA plans to invest 77 billion US Dollars for U.S. Department of Transportation from the President's Budget (U.S. Department of Transportation 2016). USA has 6,000,000 km of roads, which is the biggest road network compared to other countries (Schnebele et al. 2015). In Turkey, for the year 2016, 12 billion Turkish Liras

are allocated for General Directorate of Highways (KGM) considering all transportation activities in the central government budget law (T.C. Maliye Bakanlığı Bütçe ve Mali Kontrol Genel Müdürlüğü 2016).

Decision strategies for pavement maintenance activities are directly built upon the outcomes of Pavement Management Systems (PMSs). In order to achieve a properly functioning PMS, the current conditions of in-service pavements need to be continuously monitored and evaluated as pavements can deteriorate with time due to combined effects of continuous traffic loading and environmental effects. Pavement distresses are main indicators of the resultant damage, which can show themselves in the form of cracks either along the surface of the pavement and/or through the depth of pavements. Therefore, having a precise assessment tool for monitoring pavement cracks is an essential component of a PMS.

Evaluation of pavement conditions is accomplished either at regular intervals or after disasters. In most US states, agencies monitor pavement surface distress at one, two, or three year frequencies (Kenneth 2004). These assessments assist transportation agencies to estimate the future conditions in terms of supporting an investment plan and allocating maintenance and repair resources. If pavements are not repaired at the right time, costs may increase dramatically. As mentioned in a state of the art review study for pavement management and assessment by Schnebele et al. (2015): “The cost of reconstruction of a deteriorated road due to lack of maintenance may be more than three times the cost of preserving a frequently maintained road”.

Determination and evaluation of pavement cracks have been generally accomplished using so-called “manual inspections” that are regularly performed. This procedure typically involves a pavement condition survey form written out by a trained practitioner of a highway agency who travels along the road and collects both visual and quantitative data from the pavement surface by investigating the cracks with bare eye. Although traditional manual inspection methods are the common form of practice, they can have various problems. From reliability point of view, the manual inspection methods include natural bias as the major conclusions are taken based on the

practitioner's point of view, which is generally dependent the educational and expertise level of those people. From practical point of view, they are not only monotonous but also inefficient as it takes too much time to process the pavement data and make judgements about pavement condition. Finally, these methods usually require efficient management of trained experts, which may bring additional constraints considering the worker safety regulations as these people are under the continuous risk exposing themselves to daily traffic.

The above mentioned disadvantages and the penetration of technology with the advancement of knowledge in Pavement Engineering pushes the manual methods to leave their places to more modernized techniques, which are generally referred as autonomous pavement crack identification systems. Although many transportation agencies are investing more on automated and smart pavement monitoring systems, there is not a unique widely-accepted automated system used by all agencies to monitor the pavement surface defects. According to NCHRP synthesis published by Kenneth (2004) in the USA, nearly 20% of highway agencies started to use automated and semi-automated pavement crack identification systems. Within this context, various research studies have been made to develop such systems in the last two decades. Based on their research focus, the studies for developing a robust automated crack identification systems are generally categorized into two: (i) development of autonomous image collection systems, and (ii) advancements in designing accurately working image analysis algorithms.

The studies related to both of the above groups work towards developing an efficient pavement crack identification system and their achievements are actually dependent on each other. In the first group, line-scan and area-scan cameras are extensively utilized for processing the collected pavement images online or offline. In addition, the use of 3D laser sensing techniques can be counted in this group as part of automated pavement image collection systems. Acquiring high-resolution images of pavement surface in all three directions helps to develop better algorithms for researchers to extract pavement distresses. Such new technologies may be used to obtain fully automated systems for complete surveys of surface distresses. However, the use of

these 3D data acquisition systems are generally expensive and the processing of their data takes really long time, which may not be very feasible considering the demand for quick pavement evaluation. In the second group, the advancements in pattern recognition and/or machine vision techniques are emphasized. As widely used crack detection algorithms have certain drawbacks or limitations, the developments in this group usually focuses on new image processing algorithms. The main difficulties encountered in this group can be due to various rationales such as complex and irregular texture of cracked surfaces, having non-uniform background illumination apparent in the images, and presence of non-crack features, etc. Those challenges in an effectively working pavement crack identification system still need to be solved successfully to create an accurate, robust and timely working system, which can be used reliably as part of a modern Pavement Management System.

1.2. Objectives of the Research

The main objective of our study is to realize a robust pavement crack identification system. Within this context, such a system can only be built up with a properly working data collection platform together with data processing methods. Therefore, the objectives of this research can be divided into components as follows:

- For the data collection tool, this study aims to effectively use one of most recently introduced technology, Unmanned Aerial Vehicles (UAVs) which operates to take images from the surface of pavements.
- As part of the data collection, through the use of UAVs, this study aims to form a new pavement crack image dataset formed by collecting crack and non-crack images.
- For the crack detection algorithm, the proposed method should be able to use images taken by UAVs, on which conventional digital image processing techniques can be applied first. With this aim in mind, image enhancement algorithms including non-uniform background illumination correction, and the

removal of noises are performed and crack regions are extracted from the images using automated thresholding based image segmentation algorithms.

- With the properly detected crack candidate regions, the objective is to classify the candidates using an efficient machine learning technique called Support Vector Machines (SVMs). For this purpose, an SVM model is trained using geometric properties of crack candidate regions and then unknown candidate regions are categorized into four classes: longitudinal, transverse, alligator and non-crack.
- This study finally aims to test the performance of the proposed system using a field study where images from the real field conditions are captured using UAVs, to see whether the cracks are detected and classified correctly or not.

With the above objectives, the schematic representation of proposed pavement crack identification system is given in Figure 1.

1.3. Scope of the Thesis

In this study, we propose an automated pavement crack identification system using UAVs, in which we perform image processing methods and apply machine learning techniques to properly identify pavement surface cracks. The proposed system can be used for classifying the three most commonly encountered crack types: (i) longitudinal, (ii) transverse, and (iii) alligator cracks. Moreover, it also has an ability to label non-crack features.

The proposed system is mainly designed for classifying cracks on flexible pavements, although it is also applicable for cracks on concrete pavements, as the crack segmentation algorithm is developed in an automated manner, i.e. without the need for an expert choosing settings according to different types of the pavement.

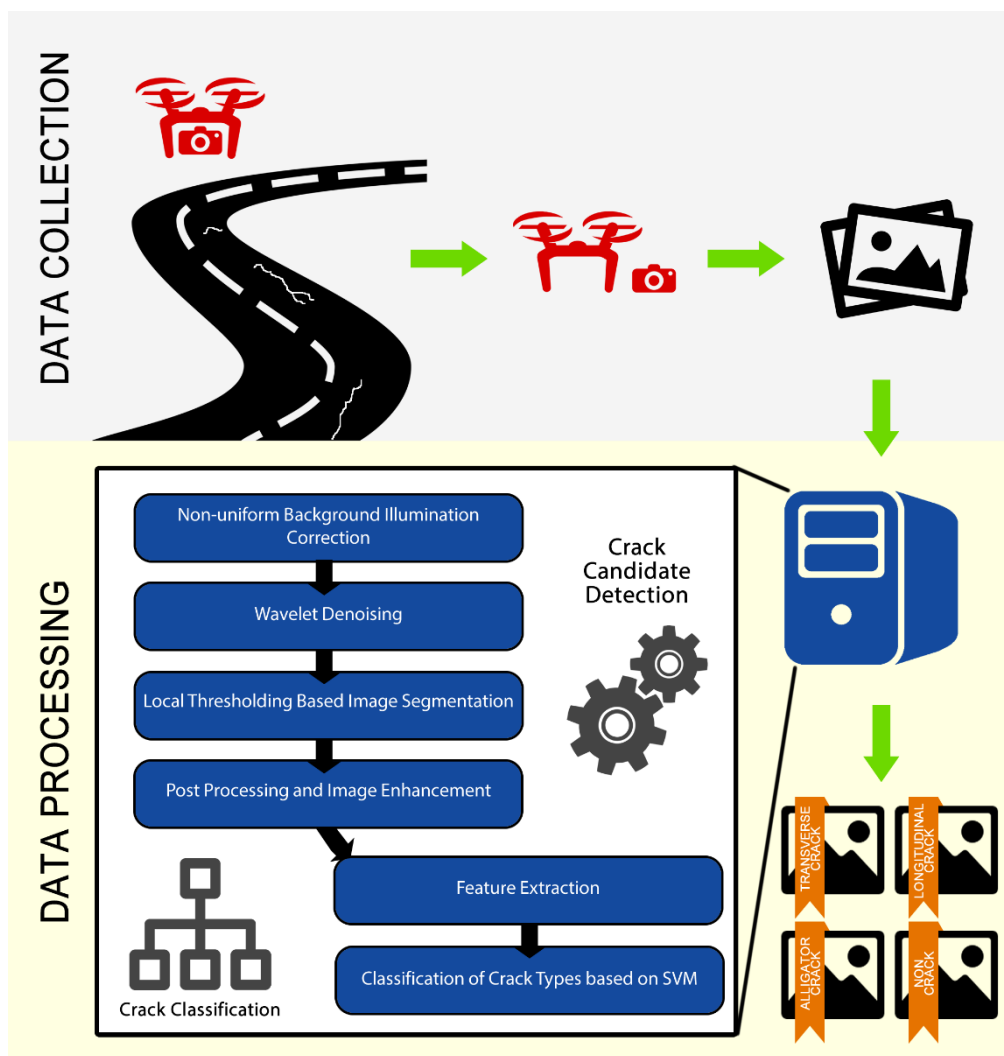


Figure 1 - Schematic Representation of the Pavement Crack Identification System

There are many data collection platforms available for conventionally used PMSs. They vary from the simplest devices such as conventional cameras to most sophisticated ones such as laser scanners. However, in the scope of this study, as data collection tool, only UAVs are considered because of their continuously growing use and improving technologies.

1.4. Thesis Organization

Considering the statement of problem, objectives of the research and its scope, the rest of the thesis is organized as follows: Chapter 2 introduces the current state of the art for data collection platforms and pavement crack identification algorithms, which also includes the essentials of UAVs including its equipment and capabilities to describe their potential in various applications. In Chapter 3, the details of proposed pavement crack identification method, i.e., the system architecture and algorithm implementations, are described. In Chapter 4, the proposed method is applied to the sample dataset obtained from a field study where Middle East Technical University is selected for the test bed. Moreover, crack identification results are presented with a discussion on the method's drawbacks and limitations. Finally, the last chapter summarizes and concludes the study, presenting future works.

CHAPTER 2

LITERATURE REVIEW

In the last two decades, the technological advancements in pavement evaluation tools have gained much attention due to increasing needs for development of fully automated Pavement Management Systems. Many studies have been made on those systems with varying accuracies. Pavement inspection systems can be categorized into two parts as (i) data collection, and (ii) data processing. In data collection part, the information from the pavement surface is gathered as 2D images or 3D surface data by using moving vehicles or aerial platforms. In addition to these platforms, manual inspections are still in-use by walking on the roads and carrying out visual inspection. After performing field experiments and collecting data, in general, the gathered data are processed using sophisticated image processing algorithms and machine learning techniques. Within the above context, this chapter presents the current literature of the data collection platforms and data processing techniques.

2.1. Data Collection Platforms

Pavement distress data can be collected in various ways. First and the oldest way of gathering pavement distress information is by walking along the road and measuring the required parameters through manual inspection. Since this method is time consuming and does not produce satisfactorily accurate results, with the help of technological advancements, automated pavement data collection systems are

developed. Nowadays, one of the most popular data collection systems is camera-mounted trucks. They are widely used in pavement inspection systems. However, the initial cost of developing such truck based systems is relatively more expensive. Because of that, researchers are looking for different ways of collecting pavement distress information. At this point, emerging unmanned aerial platforms enter into the picture as they are cheap and easy to operate. In the following sections, manual and vehicle based methods are discussed in detail.

2.1.1. Manual Inspection Methods

In the past, determination and evaluation of pavement cracks have been generally accomplished using so called “manual inspections” or “walk and look measurements”. In this procedure, a pavement expert travels along the road and collects both visual and quantitative data from the pavement surface by investigating the cracks with bare eye (Figure 2).



Figure 2 - Manual Inspection Methods in the Field (Fresques 2009)

To quantify the inspection regarding walking surveys, in the scope of Long-term Pavement Performance Program (LTPP), Miller and Bellinger (2003) provided a comprehensive pavement distress identification manual named “Distress Identification Manual”. Photographs and drawings of the distress types are given in this manual. Measurement methods for the size of distresses and definitions of the severity levels are also given in this document to provide a reference for comparison purposes. In addition, sample forms are available to record the data and report them. Therefore, visual inspections and measurements in the field can be easily performed according to this manual.

Although traditional inspection methods are the common form of practice, they have various problems. From reliability point of view, manual inspection results are highly subjective since they are obtained based on the experts' point of view, which is generally dependent on their educational and expertise level. Another issue is that, the personnel walks over the road in the traffic to rate the pavement condition, which makes the inspection procedure dangerous. Lanes should be partially or fully closed when inspection is performed, which is most of the time not suitable or sometimes even impossible. The weather during the inspection day is also an important factor to start an inspection; it should be warm enough to work. In short, from practical point of view, manual inspections are time consuming and they require plenty of time to complete even for a short road.

Since automated detection methods are faster and easier, the shift from manual inspection to modernized data collection and processing has raised over the last 20 years to speed up the assessment process. Numerous transportation agencies are currently investing for automated systems (Schnebele et al. 2015), where recent state-of-the-art technologies in computers and digital image processing techniques are mostly used and provide valuable results for pavement condition monitoring.

2.1.2. Truck Based Systems

To speed up the process of pavement conditions' assessment, cameras attached on modern vehicles such as trucks and vans are operated rather than walking on the roads. Recent developments in computer technology provide autonomous methods to gather and process the required data. Using these methods, continuous and high resolution data can be collected at high speeds. Several approaches are available for identifying different distress types on pavement surfaces, some of which are explained below.

Fukuhara et al. (1990) developed a system mounted on a vehicle that makes automated surveying of pavement distress. Although, the survey vehicle was travelling at a speed of 60 km/h to measure cracking, the maximum resolution was acquired at the speed of 10 km/h. The system was able to measure three types of distress factors; cracking, rutting and longitudinal profile. They illuminated the road surface with argon laser light and scanned the surface through a laser scanner. On the other hand, the profile data were recorded in video.

Since Roadware Corporation announced the WiseCrax system in the mid of 1990s (Klassen & Swindall 1993), it became the most widely reported system among the automated ones. The vendor describes the system as: "WiseCrax analyzes the pavement image video tapes from the Automated Road Analyzer (ARAN)". It could detect cracks; and classify them according to their types, severities and extents. In addition, it could generate crack statistics report and crack maps. The data collection process was performed by two synchronized cameras with an illumination system as illustrated in Figure 3. Each camera covers about half-width of a pavement lane. The data processing was achieved after the data collection part with some operator assistance. The vendor mentioned some restrictions of the WiseCrax system. First, data processing part was regulated by the image quality and resolution. Second, smallest crack width that can be identified was roughly 3 mm or 1 pixel wide. Lastly, some types of pavement surface such as chip seals caused insufficient crack visibility. Since algorithm could not detect those features, they had to be assessed with human involvement. Wang and Elliot (1999) conducted an evaluation of the WiseCrax

technology. In that study, they reported large differences between the outcomes of WiseCrax and manual inspections. The problem was about classifying and quantifying cracks. They noted that the difficulty of crack identification has been a research area for years, therefore the difference was not due to vendors' methods. After this study, Groeger et al. (2003) evaluated the implementation of the WiseCrax system in Maryland and they concluded that automated crack identification in a network level is possible and practical. Nevertheless, Quality Control /Quality Assurance (QA/QC) procedure must be strictly followed to accomplish reliable and sustainable results.

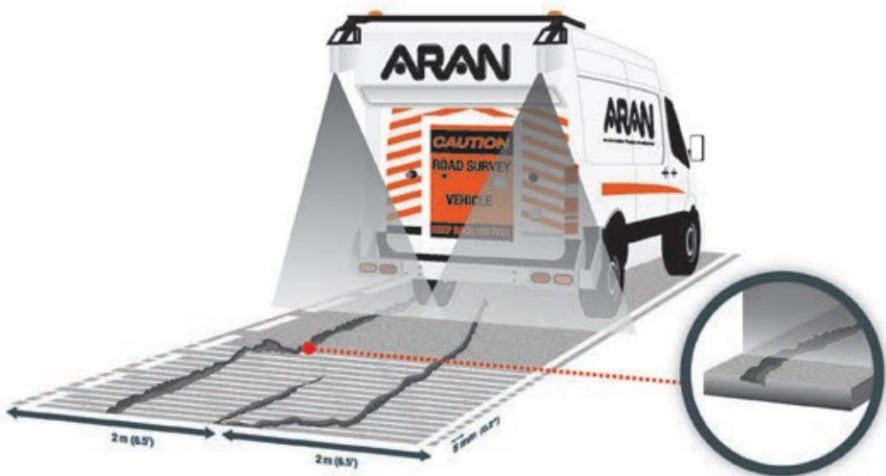


Figure 3 - Automated Road Analyzer Vehicle (Klassen & Swindall 1993)

Wang et al. (2002) introduced on the University of Arkansas Digital Highway Data Vehicle (DHDV). The data mentioned in this study was collected and manipulated in real time on a 4.5 km section of a highway. The driving speed was changing from 32 to 64 km/h. The imaging was performed at night with a frame-based digital camera and four strobe lights to illuminate the roadway to increase the image quality. The exact location of the vehicle was acquired through the use of a Global Positioning System (GPS) tool which records data to the database. The importance of the research was the processing of images performed on real-time. Data processing system was

embedded in on-board computers of the vehicle, which was a multicomputer and could perform multi-CPU-based parallel computing.

In another study, an automated real-time distress analyzer was reported using DHDV to collect high-resolution images and identify cracks (Wang et al. 2003). The data used in this work covers a network of approximately 100 miles of pavements. Compared to the previous works, the acquisition system had 2 times greater resolution than the previous one, and it included an additional improvement for image processing algorithms such as more accurate determination of lane marking. The authors anticipated that the use of automated pavement surveying systems would be real in the following years.

In 2006, a semi-automated distress surveying system was announced by Salvatore Cafiso and Battiato (2006). The purpose of the study was to increase the safety and reduce the labor cost requirements. Geo-referenced digital images were collected using a digital camera, attached on the back of the Mobile Laboratory developed by the Department of Civil and Environmental Engineering of Catania University. With the purpose of limiting costs, the system did not have any illumination lamps. The problems connected to daylight illumination difference was tried to be solved in the detection algorithm. Pavement Distress Analyzer (PDA) software was utilized to automatically detect cracks, potholes and patches which are then classified by an operator. Since the Mobile Laboratory could not travel at very high speeds (25-30 km/h), the procedure was feasible for local road network as part of a Pavement Management System.

Sy et al. (2008) introduced a real-time processing method used for road characterization named as AMAC, in France. Data acquisition was achieved with two line-scan cameras and two laser illuminators mounted on AMAC. The vehicle could travel at average speed of 80 km/h. The size of road captured by each image was 3.9 m x 4 m. Crack detection part was accomplished offline and manually by an operator observing the images on a monitor. The authors mainly aimed to detect absence of cracks on road surface through image processing to lower the number of images

observed by the operator. The results of this technique and processing time showed that the method is well and fast enough to classify images in real time.

In Spain, Gavilán et al. (2011) developed a system to handle automatic road distress assessment completely, which consisted of an online image recording and an offline image processing stages. Similar to previous methods, the vehicle had line scan cameras with 2000 x 1 pixels resolution covering up to 4 m x 1 mm of the road. In the pre-processing stage, the texture was smoothed and linear features were enhanced. Then, a seed-based method was performed to identify cracks, combining Multiple Directional Non-Minimum Suppression (MDNMS) including a symmetry check. Finally, a linear SVM classifier was trained to separate up to 10 different types of distresses. To obtain the optimal feature vector, different texture-based features were used. Then all parameters were optimized depending on the output of the classifier. The result of crack detection system was significantly dependent on parameters changing with type of pavements.

After decades of research studies for pavement distress detection, a fully automated method with two-dimensional (2D) data collection system continues to be a challenge under different illuminations and low resolution images. To propose a different approach, a three-dimensional (3D) laser system that can store 3D elevation of pavement profiles instead of 2D data came into the market including improvements for sensor technology. Tsai and Li (2012) published an article, which reviews the possibility of using emerging 3D imaging technologies for crack detection under different illumination and low intensity contrast environments. They integrated a sensing vehicle for acquiring 3D pavement surface data at the Georgia Institute of Technology. The system including two laser profiling units, was mounted on the vehicle to cover full lane's width as shown in Figure 4. Each profiling unit contains a laser line projector, a filter and a camera. The resolutions in x (transverse profile direction) and z direction were approximately 1 mm and 0.5 mm, respectively. On the other hand, the maximum resolution in y direction was influenced by the distance measurement instrument (DMI) and the encoder. Transverse profiles at 4.6 mm could be collected with a speed of 100 km/h. Figure 5 illustrates the collected 3D data from

the pavement surface at a close look. Controlled and actual tests were established under various illumination conditions and low resolutions. The preliminary results of controlled tests showed that cracks with at least 2 mm width could successfully be segmented from the pavement background. That means pavement crack detection with 3D laser imaging was very promising compared to 2D technologies. Tsai et al. (2015) introduced later study using same 3D line laser imaging technology on airport runway shoulders in 2015. As a new feature, the authors employed cost estimation that depends on the crack length in each crack category using varying crack sealing methods. A case study was carried out on a 30.5 m runway shoulder of an airport. The results indicate that, the proposed approach was capable enough to provide an automatic approach to generate categorized crack maps and estimate crack sealing cost.

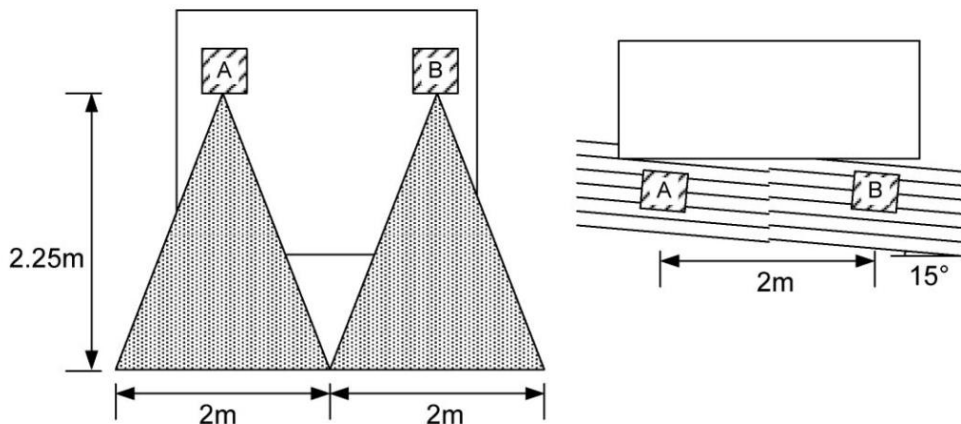


Figure 4 - Laser Crack Measurement System and Projection of Laser (Tsai & Li 2012)

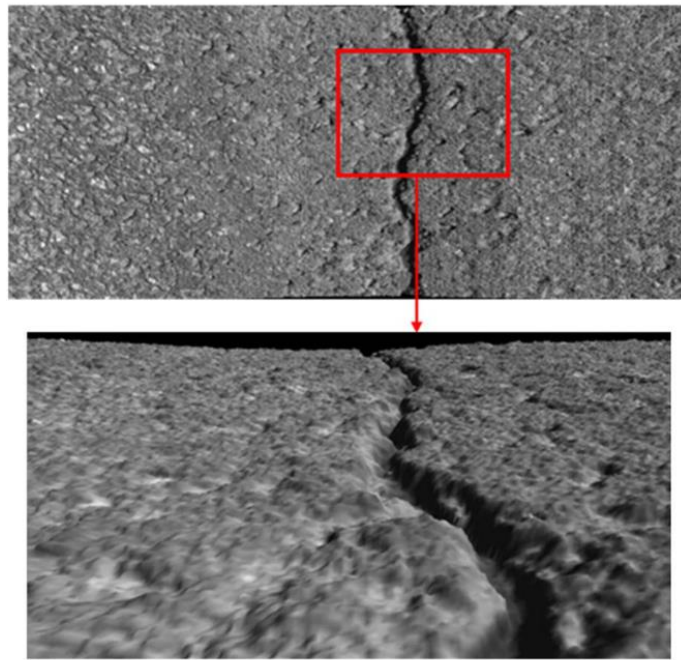


Figure 5 - Visualization of 3D Pavement Surface Data (Tsai & Li 2012)

2.1.3. Unmanned Aerial Vehicles

Satellite images are primarily used as input data for observing after effects of natural disasters, however, such images cannot be gathered in a few days after the disaster. In contrast, Unmanned Aerial Vehicles (UAVs) are able to offer high resolution and almost real-time images often cheaper than other space born platforms.

A UAV, so called a drone, is an air vehicle which can fly without a human pilot. UAVs started to be used by military reconnaissance purposes in the 1950s. For the duration of the cold war, several countries launched projects with the purpose of manufacturing vehicles that can be used for reconnaissance, surveillance and penetration of hostile territories missions, without the existence of a pilot. However, in the last decade, they have become extremely popular especially in civilian applications because of its low cost and practicality. With the advancements of its technology, newer commercial UAVs come to the market more frequently. With every addition, robustness and

reliability of these device also improve. These improvements make UAVs a more trustworthy way for photography. Moreover, with the increasing capabilities of the on-board GPS systems, most of the UAVs even support autonomous flight up to some level of freedom. UAVs are equipped with various sensors, including gyroscope, magnetometer and accelerometer to detect 3D orientation and GPS sensor for navigation. Some UAVs also include vision-positioning system, which makes use of a low-resolution camera directed to the ground to detect small movements at low altitudes, and a sonar system to identify altitude in areas where GPS-acquired altitude values are inaccurate, and even to avoid collusions automatically in either autonomous or pilot-controlled flights. Moreover, UAVs can be equipped with different payloads such as factory mounted camera systems, external cameras, and infrared sensors, etc.

UAVs can be categorized in two ways, namely, fixed wing (Figure 6a) or rotary wing (Figure 6b). Among these, commercially used UAVs are often rotary wings and more specifically they are multicopters such as quadcopters, hexacopters or octocopters. This is mostly because they are more stable in-air compared to helicopters and their better ability to vertically takeoff and land in contrast to the fixed wing UAVs. Among the multicopters, quadcopters are the most popular ones, because they are smaller and easier to carry around. However, octocopters and hexacopters have redundancy, i.e., in the case of single or even multiple rotor failure device can adjust to the momentum changes without crashing. These UAVs can carry heavier payloads. Cameras on UAVs are often combined with gimbals to get more stable images. Gimbals have their dedicated Inertial Measurement Unit (IMU) to adapt the cameras to the movements of UAV during the flight by changing the camera orientation using their motors. Gimbals have dampers to reduce the effect of in-flight vibration to ensure that images can still be reliably captured while the UAV is moving.

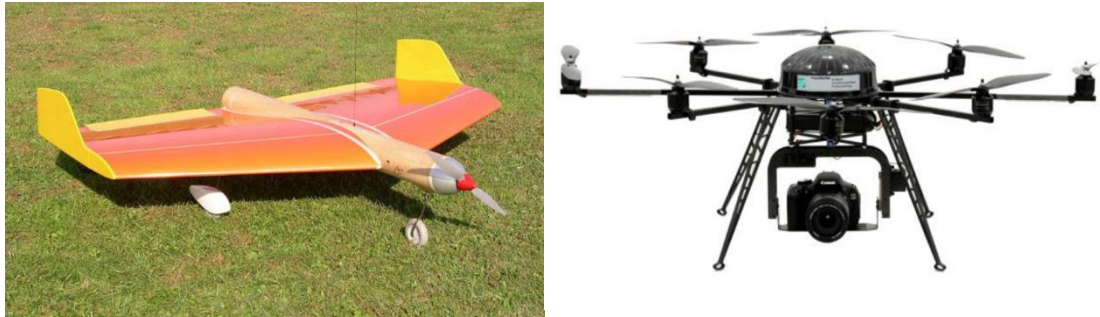


Figure 6 – Type of UAVs (a) Fixed Wing (Bendea et al. 2008) (b) Rotary Wing (Eschmann et al. 2013)

The UAV platforms provide economic, superior flexibility, shorter response time and capture high resolution data compared to traditional platforms. In contrast to truck mounted camera road monitoring systems, they are cheap and easily transportable. UAV systems are capable of capturing images of road and vehicles within 2 hours of the event to provide information about traffic, accidents or natural disasters in a cheaper way than conventional aerial vehicles (Feng et al. 2009). Manual methods and truck-based methods may cause traffic disruption due to traveling in a slow speed. However, emerging remote-controlled UAVs can fly over a certain height not to interrupt the traffic flow. This makes UAV systems a good practical solution under the heavy traffic (Koch et al. 2015).

With their increasing accessibility and ease-of-use, various applications of UAVs were presented in the literature. Among those, the research studies related to our work are given in this section. For example, Bendea et al. (2008) developed a cost effective aerial platform with a photogrammetric payload for use after natural and manmade hazards to detect and classify structural damages. The UAV had to be easily transportable and autonomously usable. Therefore, they mounted an autopilot board to the aerial platform that allows scheduling flights at planned positions. The configuration of the UAV included onboard digital sensors to collect image and video. A number of test flights were carried out to estimate flight performance of the platform and to check the linkage between the autopilot board and the payload. Rather than presenting a solid conclusion, the authors mentioned ongoing developments about in-

flight position accuracy and photogrammetric processing of the acquired data. In another study, Tatham (2009) summarized the needs for assessment processes, capabilities and cost of the UAVs and explained barriers against their use in response to a disaster. Accordingly, the use of UAVs offers advantages over the use of manned aircrafts because of their flexibility and comparative low cost. Nevertheless, aerial surveillance is mostly dependent on the type of the disaster and related topography. For example, UAVs are more likely to be successful in mountainous areas where there are not enough facilities to take off/landing for manned aircrafts. Like many developing technologies, given that the cost of designing and using a UAVs is reducing while their capabilities are increasing every day. It was not evitable that UAVs can aid in the response to a disaster.

UAVs with proven performance in natural disasters led them to be used in structural health monitoring. Eschmann et al. (2012) reported a study at Fraunhofer IZFP, Germany where they scanned a building for inspection purposes using a digital camera mounted micro air vehicle (MAV). The developed MAV had microcontroller-based flight control system and various sensors for navigation and flight stabilization. An octocopter, a configuration of eight rotors, was selected to preserve a significant level of safety in case of failure of one or more electric motors. For data collection, the digital camera was programmed to take 3 pictures per second by an automatic photo-firing system. Those pictures were stored in the main board of the vehicle. 12,000 images were taken for four days of flight, several hundred images were stitched to create a full 2D image of facade (Figure 7). To handle large picture size, the model was separated into parts of 10 window frames each. For crack extraction, an edge detection method was implemented based on applying a Gaussian Blur to the original image than subtracting it from the same image. That method was reported to be developed further in the future as it performed better results for larger scale damages, although tiny surface cracks were not visible after image processing application.



Figure 7 - Process For Facade Modeling (Eschmann et al. 2012)

Ellenberg et al. (2014) applied image-based crack detection for masonry wall using a UAV and discussed the major challenges. The major problem to use a UAV for visual inspection was flight control in extreme environmental conditions. Wind was an enormous challenge. If the wind speed was higher than 10 mph, it took the UAV away from the planned path. The best solution of this challenge was to only use the UAV in appropriate wind speed levels in between 5 and 10 mph. Another notable challenge was the registration of picture to the GPS coordinates. GPS recording could be imprecise caused by restriction of structures. To increase the GPS recording accuracy, the UAV had to stay farther away from the structure. The authors did not mention the resolution of images. As UAV moved away from the structure, the detection of cracks became challenging for low resolution images. In conclusion, the authors engaged to perform a future test and concluded the study with explaining the potential of UAVs for infrastructure monitoring in the future.

The first road condition assessment using UAV was introduced by Zhang (2008). The flights were done by a radio controlled low cost airframe helicopter equipped with position and velocity detection sensors. The weight of the device was approximately 6.1 kg and UAV was able to carry a payload of almost 6.4 kg. It can fly approximately

30 minutes carrying full payload. Several field tests were performed to collect imagery of unpaved roads with various defects. Data processing part includes camera calibration, extraction of model of 3D road surface and orthoimage generation. The structure of proposed system is illustrated in Figure 8. A number of image processing algorithms are under development to calculate some features such as length and size of corrugation, geometry of cross section, rutting, potholes etc.

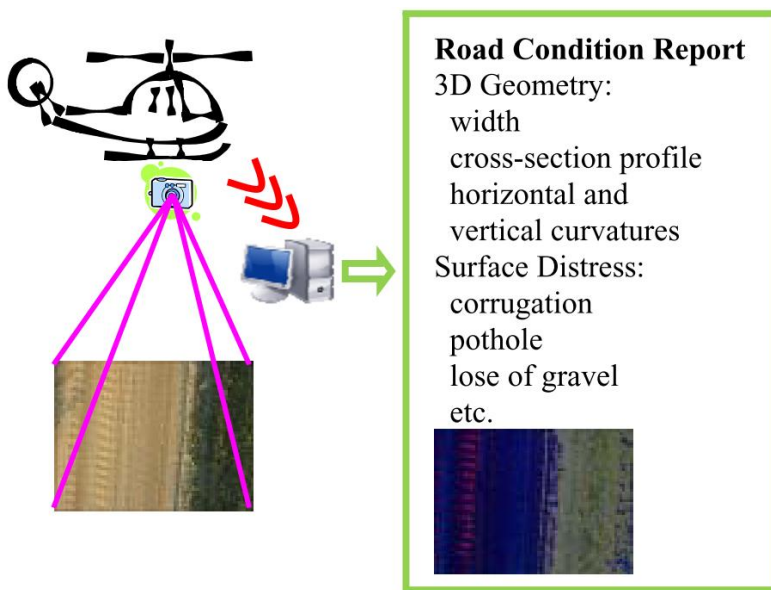


Figure 8 - Proposed UAV-Based Remote Sensing System For Unpaved Road Condition Assessment (Zhang 2008)

Feng et al. (2009) presented a real-time road mapping system to calculate the geometric properties of the road. In this system, a fixed-wing UAV with double engine was operated. Different from other studies, the vehicle was equipped with a parachute to improve security of the system. The gross weight was 40 kg. This device was capable of flying at a speed of 50-100 km/h for 2 hours within 20 km radius. A digital camera was mounted on the system with a stabilizer in three-axis. An experiment was carried over above a freeway in a sunny and not much windy day. Continuous images of the road were produced in which vehicles can be detected and number of vehicles

can be calculated automatically (Figure 9). Aerial images taken from 20 km radius area could be gathered in 2 hours, which makes the system very useful in a natural disaster. The deficiency of the system was that it may not be suitable for large scale operations. In the experiment, no Ground Control Point (GCP) was used. The authors mentioned if some GCPs could have been adopted, the accuracy of the calculations would have been much higher.

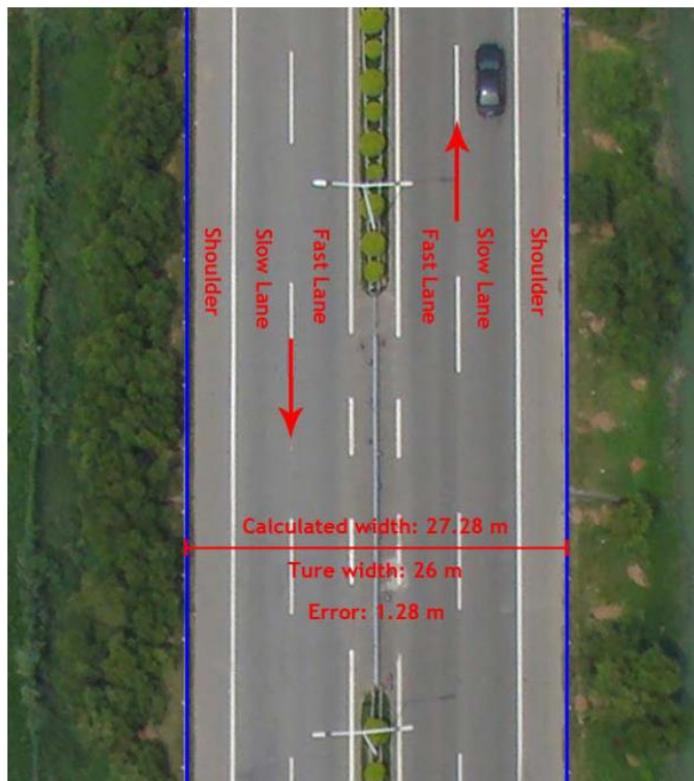


Figure 9 - Road Information Detected by this System (Feng et al. 2009)

Zhang and Elaksher (2011) published a study where an improved form of UAV-based road condition assessment was performed. The new system included a low-priced model helicopter armed with a 10.1-megapixel resolution digital camera, a GPS receiver and an Inertial Navigation System (INS) and Ground Control Station (GCS). The 6.8 kg mini UAV has 25 minutes flight time 200 m above the ground. A flight

mission software was installed on a GCS computer that allows mission planning including parameter settings such as way points, altitude and speed of the UAV. The ground resolution up to 5 mm was obtained from a UAV flight at 45 m altitude. To obtain more accurate measurement for the road surface distress, new set of algorithms were developed for generation of 3D surface model and orthoimages. A new strategy was introduced to efficiently investigate the image geometry to maximize the matching accuracy and to reach the maximum 3D position precision. The reconstruction method could regenerate a 3D model of distresses as potholes and ruts only, which increases the accuracy of measurement in 3D. The difference between the 3D model and field survey data indicated that maximum accuracy could be achieved up to 0.5 cm ground accuracy using the UAVs. The results shows that the proposed system is practical for local transportation agencies to gather surface conditions of unpaved roads. Road images were collected with UAV and distress evaluation were performed in office, i.e., no fieldwork was needed. For that reason, it would be helpful for local agencies to perform quick, efficient, and safe condition assessment of rural roads.

2.2. Data Processing Techniques

Computer vision techniques become an essential part of latest Structural Health Monitoring. These methods are developed upon image processing techniques such as template matching, histogram equalization, background extraction, linear and nonlinear filtering, edge and line detection, texture recognition etc.

Digital image processing techniques are developed to separate the defects from the background image and create a binary one. The identification of crack is interpreted from this image. Wavelet and Fourier transforms as well as segmentation algorithms are the most widely used techniques utilized for pavement distress identification.

The recognition of cracks using those techniques is challenging as cracks compose a small part of the pavement image. Furthermore, the image has lots of irregularities

similar to cracks. The automatic identification of pavement stress is more complicated for images with non-uniform illumination, shadows and surface textures.

There have been numerous studies performed in this area. Huang and Xu (2006) introduced VCrack system which was a modified image processing algorithm for high-speed and real-time monitoring of pavements. The algorithm consists of three principal steps:

1. Grid cell analysis
2. Crack seed verification
3. Crack cluster connection

In the first step, the image taken from pavement surface was split into grid cells of 8 x 8 pixels to decrease the computational cost of crack identification. Each cell was categorized as either non-crack or crack cell by comparing the grayscale information of the pixels. The cell map of the pavement image was created by reducing each marked potential crack seed to one pixel.

Second, the contrast of each crack seed and its neighbor was compared to verify whether the crack is truly a part of a crack or not. If the contrast exceeds the predefined threshold value, then the crack was validated. Lots of seed that result from pavement noise could be eliminated in this step.

Finally, VCrack was used to join single seeds into seed clusters. Beginning from one seed, a crack cluster expanded by admitting neighborhood seeds one at a time until no close seed could be recognized. Three criterions were chosen to validate whether a crack seed cluster was a section of an actual crack or not: (i) the contrast of the pixels on the cluster path to the nearest pixels should not go above a threshold value not to be defined as light marks paint (ii) the band width and its variation should be in the acceptable limits to get rid of shadows and other non-crack objects, and (iii) the length of the path must have a minimum value to differ from the pavement noise or undesirable regions. After non-verified crack clusters were removed, the remained clusters placed in parallel directions were connected to become a long crack. The

performance of VCrack was calculated by matching the results of human interpreted cracks and the cracks identified using the algorithm. The correlation was 0.91 and 0.96 for longitudinal and transverse cracking, respectively.

Zhou et al. (2006) proposed a wavelet-based method for pavement distress identification. Like Fourier Transform, wavelet transform decomposes signals into their components. However, rather than decomposing the signal into sine series, wavelet decomposes the signal into its “wavelets”. Wavelets are scaled and shifted version of mother wavelets. They are unequal in shape and compactly supported. Therefore, using wavelets is ideal for pavement distress images since they have discontinuities and sharp changes. If a pavement image is transformed to different frequency sub bands using wavelets, distresses are generally seen in the high-frequency sub bands because of their irregular shape. On the other hand, background arrives on the scene in the low-frequency sub bands.

In this study, to achieve efficient storage of distress images, a modified Embedded Zerotrees of Wavelet (EZW) coding algorithm was offered for pavement image compression. According to experimental results, the algorithm could compress pavement image more than 2%. Thanks to the EZW, noise reduction effect could also be achieved by threshold operation to avoid small wavelet coefficient from being encoded.

First the data were compressed and decoded to obtain wavelet coefficients. High-amplitude wavelet coefficient percentage (HAWCP) and high-frequency energy percentage (HFEP) were determined as measures to identify distresses and isolate them from the pavement images. Then Radon transform was applied for easier distress classification. Then, quantification norm was established to evaluate pavement conditions. Remarkably, every part of the proposed method: distress identification, image compression and noise reduction were developed in the frequency domain. Compared to manual inspection methods, the introduced approach has benefits such as being fast, automated and appropriate for different pavement types and stresses.

Oliveira and Correia (2009) presented a simple unsupervised system for detection and isolation of cracks in pavement images acquired during the road surveys, and their classification into a predefined set of crack classes. Two distinct databases were used for testing, first one was collected using high speed acquisition system (DB1), second one was acquired during human observation survey (DB2). The proposed system architecture is shown in Figure 10.

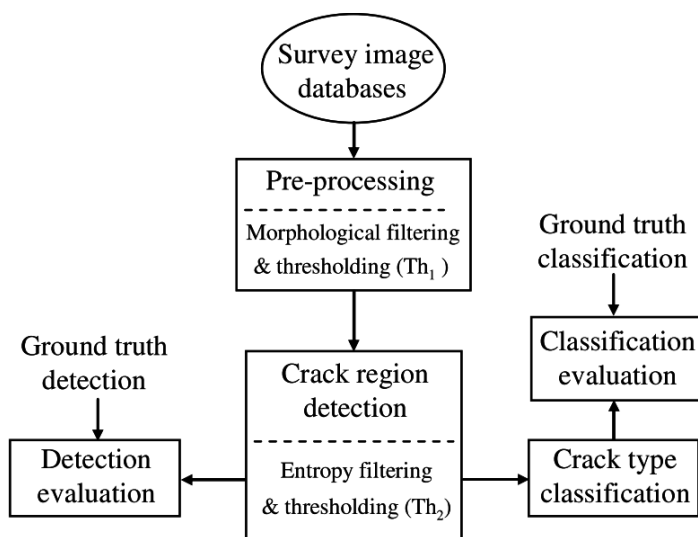


Figure 10 - System Architecture For Crack Detection and Classification (Oliveira & Correia 2009)

For each database (DB1 and DB2), different pre-processing strategies were adopted to adjust non-uniform illumination. After normalization, a popular morphological operation was applied for all images to decrease the intensity variance as in Equation (1):

$$\text{Img} \circ se = (\text{Img} \ominus se) \oplus se \quad (1)$$

where the symbol \circ represents the morphological opening operation, \ominus denotes the morphological erosion while \oplus stands for the morphological dilation. se represents a structuring elements which looks like a disk shape. After morphological operation, further normalization step was applied. A dynamic threshold value, Th_l , was needed to be calculated, as given in Equation (2).

$$Th_l = Th(Ot) - 0.5 \times std(Img) \quad (2)$$

where $Th(Ot)$ is the threshold value computed according to modified Otsu method using only the intensity levels lower than a mean intensity level for each image. $std(Img)$ is the standard deviation of all image pixel intensities. The output of thresholding operation was a binary image where the pixels with value 0 means non-crack pixels and the ones with value 1 means potential crack pixels.

After applying the threshold Th_l , the binary image block was separated into non-overlapping blocks of 75 x 75 pixels. Entropy of each binary blocks $E_{binblock}$ was calculated by Equation (3):

$$E_{binblock} = |f_0 \times \log_2(f_0) + f_1 \times \log_2(f_1)| \quad (3)$$

where f_0 and f_1 are the frequency of pixels labelled with 0 and 1, respectively. Crack pixels in an image block could be measured in a faster way using entropy since entropy is invariant to the position of crack pixels in the block.

With the purpose of classifying image blocks whether they contain crack pixels or not, additional thresholding operation (Th_2) was applied, now on the entropy blocks matrix:

$$Th_2 = 0.5 \times Th(Ot)_{binblock} \quad (4)$$

where $Th(Ot)_{binblock}$ is a threshold computed using a modified Otsu method, as performed for Th_1 . After Th_2 , the resulting isolated blocks labelled with “1” were deleted. Because these blocks usually represent the noises such as oil stains in the pavement.

Once region of crack pixels detected, they can be classified into crack types: longitudinal, transversal or miscellaneous. The feature space shown in Figure 11 was used for classification. Crack classification used the standard deviation of the column and row coordinates, of the detected crack regions, i.e., image regions labelled with “1” in the detection results matrix.

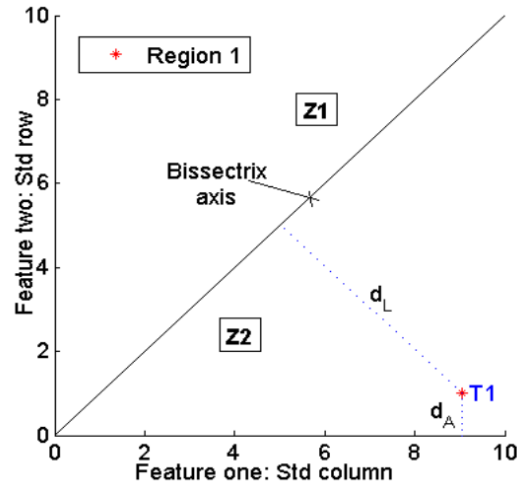


Figure 11 - 2D Feature Space Used For Crack Classification (Oliveira & Correia 2009)

Crack classification was performed by computing two distances: d_L and d_A , for each connected crack region, represented by a point in the feature space. A probability of a

crack being part of longitudinal, transversal or miscellaneous classes was calculated using d_L and d_A distances. Then the decision for a given crack type was made according to the highest probability.

The proposed method achieved 94.8% and 95.6% recall values for DB1 and DB2, respectively. The robustness of the system showed that the method is quite good in overall system performance. Moreover, a faster processing was also achieved. The system classified an image in 5 seconds for DB1 and 3 seconds for DB2.

Nguyen et al. (2009) introduced a method, which can detect cracks, joint and bridged defects (Figure 12). The proposed method had three stages:

1. Detection of lane-marking
2. Defect detection by anisotropy
3. Classification of crack types

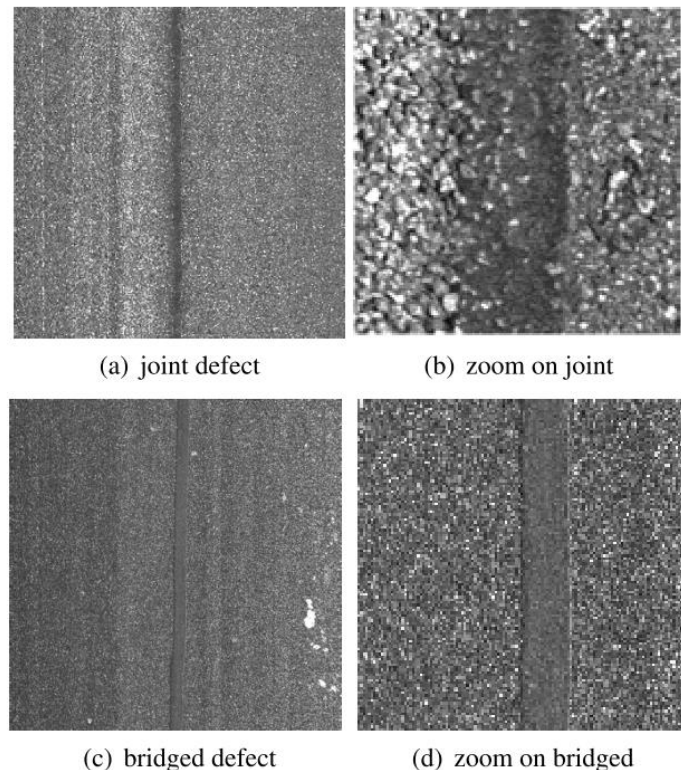


Figure 12 - Joint and Bridged Defect Sample (Nguyen et al. 2009)

To get rid of lane marking, a threshold was applied to the pavement image. Probabilistic Hough Transform was used to distinguish lines on the resultant binary image and the lane-marking pixels were not taken into account for further crack detection calculations.

Conditional Texture Anisotropy (CTA) of the image was calculated using mean and standard deviation of the whole image for defect detection. CTA takes values in between 0 and 1. If CTA value is close to 0, it means that pixel is defect free pixel. In contrast, if CTA takes high value close to 1, it is a crack pixel. Crack pixels can be easily detected by a threshold value from CTA image.

Detected defect pixels were categorized into four different types:

1. Crack (Longitudinal, transversal or alligator)
2. Joint
3. Bridged Contour
4. Defect-free region

Five different features of each class, e.g. mean, standard deviation, width of boundary rectangle, were extracted and trained using multi-layer perceptron neural network. The training set contained 150 defect free images, 100 longitudinal crack images, 87 transversal crack images, 35 alligators crack images, 100 joints and 100 bridgeds. Results of the experiments showed that the proposed method could detect cracks as small as 2 mm. However, the results of bridgeds are not as good as results on cracks and joints.

Li et al. (2011) proposed a method named as FoSA which is a seed growing method based on F* algorithm for automatic crack-line detection. F* algorithm is used to find linear features in a global view. FoSA took the advantage of F* algorithm but eliminated the necessity that the start and end points should be set beforehand. Thus, FoSA was able to identify those points automatically. The main purpose of the method was finding a path throughout the seed point and inside the image with a minimum

average path cost. FoSA was a two-step method. At first, FoSA collected crack seeds automatically with aggregating crack sections, creating crack elements and average-path-cost-based filtering. In the second step, an efficient F* Seed growing algorithm was applied to get crack string and conduct linking and pruning. The result of experiments illustrated that the suggested method was capable of removing anti-speckle-noise and obtaining crack lines with high efficiency and reliability.

Zou et al. (2012) developed a new method, called “CrackTree” to detect cracks from pavement image fully-automatically. The method had three main parts (Figure 13):

1. Geodesic shadow removal
2. Building crack probability map using tensor voting
3. Setting of crack seeds from the crack probability map

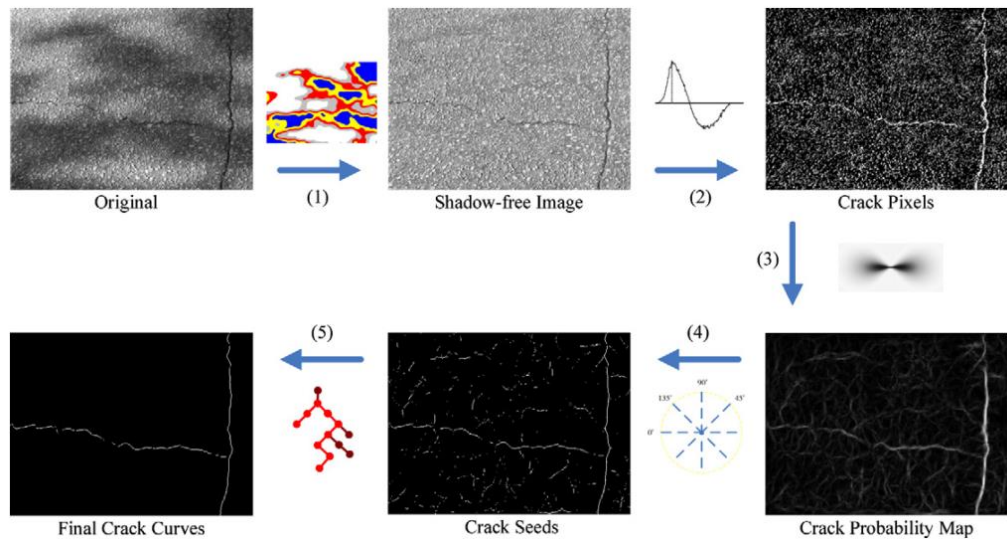


Figure 13 - Flow Chart of the Proposed Cracktree Method (Zou et al. 2012)

For the shadow removal stage, the authors applied a geodesic model to separate a shadow region into different levels since the shadow density was reduced from shadow center to shadow boundary. Then, tensor voting was employed to enrich cracks in the images by creating a crack probability map in which the probability of pixels placed

along long crack curves was enhanced. On the contrary, the probability of the dissimilar pixels to be connected to other crack fragments was eliminated. Finally, a tree representation and pruning algorithm was developed to get rid of the image noise. Minimum spanning trees (MSTs), defining the possible connections of sampled crack seeds, trimmed unwanted edges to finalize the crack curves.

To examine the performance of CrackTree, Precision, Recall and F-measure criterias were calculated by comparing the detected crack curves in contrast to the human labeled ground-truth crack curves. The proposed method reached an average F-measure of 0.85, higher than those obtained through several other existing algorithms.

Finally, Oliveira and Correia (2013) presented an unsupervised two-steps pattern recognition system, called CrackIT, for the identification of cracks in flexible pavements. First, the image blocks including crack pixels were found. Then, cracks were classified into types as defined by Portuguese Distress Catalog. The system was capable of estimating the average width of each identified crack for determining the severity level of the crack.

For crack detection purposes, non-overlapping 75 x 75 pixel blocks were chosen to decrease the processing time and required memory space. Two feature spaces in 2D were calculated for each image: the mean matrix with each crack block's average intensity and the standard deviation matrix with the corresponding standard deviation values.

Later some clustering methods were implemented to understand the crack detection compatibility. The mixture of two Gaussian models showed the superior performance with the best global error rate. The performance of the method was evaluated comparing the pavement photos acquired along a road in Portuguese, which were manually labeled by human experts, and cracks detected by proposed method. Crack identification results were acceptable. The system was able to detect multiple cracks in a single image and it took to process 56 images in about 2 minutes dealing with 2 mm wide thin cracks.

CHAPTER 3

PAVEMENT CRACK IDENTIFICATION METHOD

This chapter explains the details of the method proposed in this study to successfully detect the pavement cracks and classify them with a reasonable accuracy. The main flow of the method is inspired from the study of Gungor and Pekcan (2013) and more capable and automated version is developed in this study. The architecture of the pavement crack identification system and its algorithmic components are described in this chapter.

The proposed method has mainly two parts: (1) crack candidate detection and (2) crack classification. In crack candidate detection part, crack candidate regions are first obtained by image enhancement and segmentation algorithms. Then, the features of crack candidate regions are calculated using geometric properties for further analyses. Finally, in the crack classification part, crack candidate regions are classified into four different group including non-crack type using a properly trained Support Vector Machines (SVMs) model. Flowchart of the crack identification algorithm is given in Figure 14. Each step is explained in detail in the following sections of this chapter.

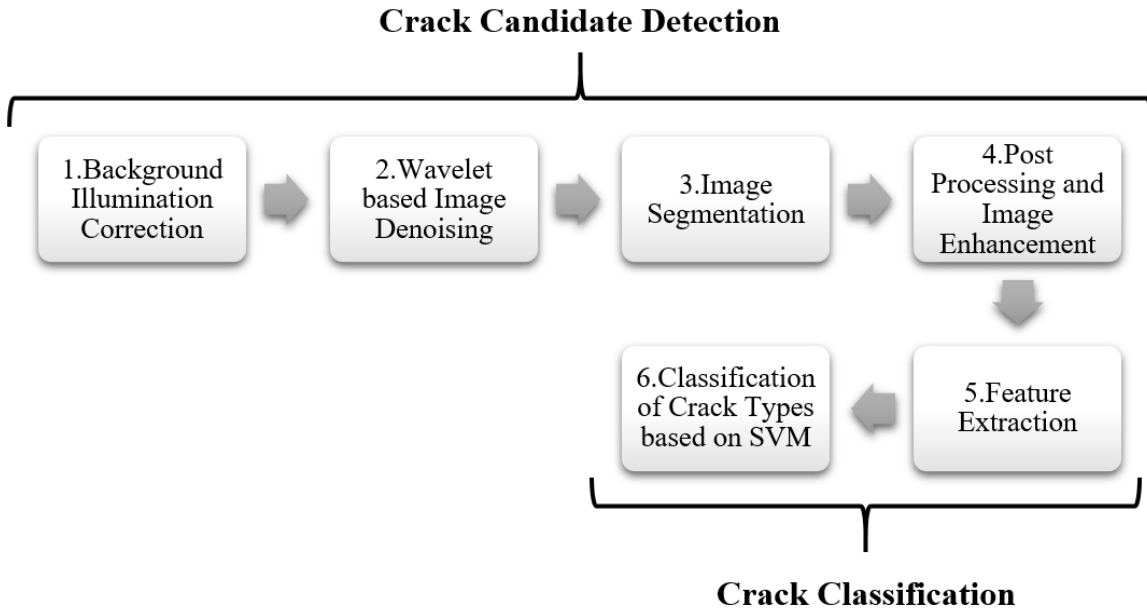


Figure 14 - Flow Chart of the Proposed Algorithm

3.1. Crack Candidate Detection

Crack candidate detection part starts with a preprocessing of the images. First, all images are resized to 512 x 512 pixels to decrease the space allocated in computer memory and consequently to speed up processing time of the algorithm. After resizing operation, they are converted to gray scale. Then, the images with non-uniform background illumination are corrected to get the same results with the uniformly illuminated ones. After that, undesired noises are removed in the frequency domain using wavelet transformation. The images are then converted back to the space domain and a threshold is applied to extract crack candidates from the background image. Finally, image enhancement operations are employed to make crack candidate regions to be processed further for the crack classification part. The details are explained in the following sections.

3.1.1. Non-uniform Background Illumination Correction

In photography, illumination is a critical issue to adjust lighting on the picture. The uniformity of illumination in a picture mainly depends on the angle and intensity of illumination resources (Zhao et al. 2010). If the light coming from the sun is not sufficient or non-uniform, additional light can be included on the photo scene to get more visible and uniformly illuminated pictures.

Since the proposed UAV system does not have its own illumination resource, it can only be used in daylight conditions. The illumination in images during daylight flights highly depends on the time of the day. To overcome the illumination problem, an algorithm is developed to ensure the same background lighting condition for all pavement images. As a result, the proposed method is expected not to depend on acquiring time as long as photos are taken during day time.

The non-uniform illumination elimination algorithm focuses on a background subtraction method which is based on morphological operations. Morphology is a popular set of image processing operations which handles images based on their shape content. Morphological operations generally apply a filter to an input image and create an output image. The value of each pixel in the output image depends on an assessment of the corresponding pixel in the input image and its neighbors. The output is very sensitive to size and shape of the selected filter. The most widely used morphological operations are dilation and erosion. While dilation adds pixels inside the filter, erosion removes the ones within the filter. Although, morphological operations are frequently used on binary images, in some cases they can also be applied to grayscale images, since grayscale erosions and dilations give similar results as the non-linear minimum and maximum filters (Salari & Bao 2010). Details of morphological operations used in binary images are discussed in the following sections of this chapter.

In order to extract non-uniform illuminated background, first erosion and then dilation operations are conducted as represented in Equation (5) where \ominus denotes erosion and

\oplus denotes dilation. As a filter type, disk-shaped filter is selected, the geometry of a representative filter is shown in Figure 15.

$$\text{Img}_{\text{background}} = (\text{Img}_{\text{grayscale}} \ominus se) \oplus se \quad (5)$$

The morphological operation eliminates the small objects as cracks in the foreground while preserving the background. In this manner, the non-uniform illumination of background can be obtained effectively. Then, the non-uniform illumination effect is fully removed by subtracting background from the grayscale image:

$$\text{Img}_{\text{uniform_illumination}} = \text{Img}_{\text{grayscale}} - \text{Img}_{\text{background}} \quad (6)$$

Last, the average intensity of the background image is added to every pixel of the obtained image to ensure more realistic and uniformly distributed background. The results of the above operations are summarized in Figure 16. Figure 16a provides an example image taken from the surface of the pavement. Non-uniform illuminated background extracted by morphological opening operation is provided in Figure 16b. Figure 16c illustrates the intensity surface of the background in 3D space. The resultant image after the removal of non-uniform illumination effect is given in Figure 16d.

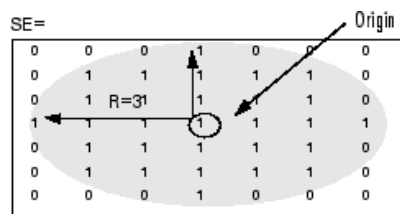


Figure 15 - A Disk Shape Filter Where the Radius is 3 Pixels (Mathworks 2016)

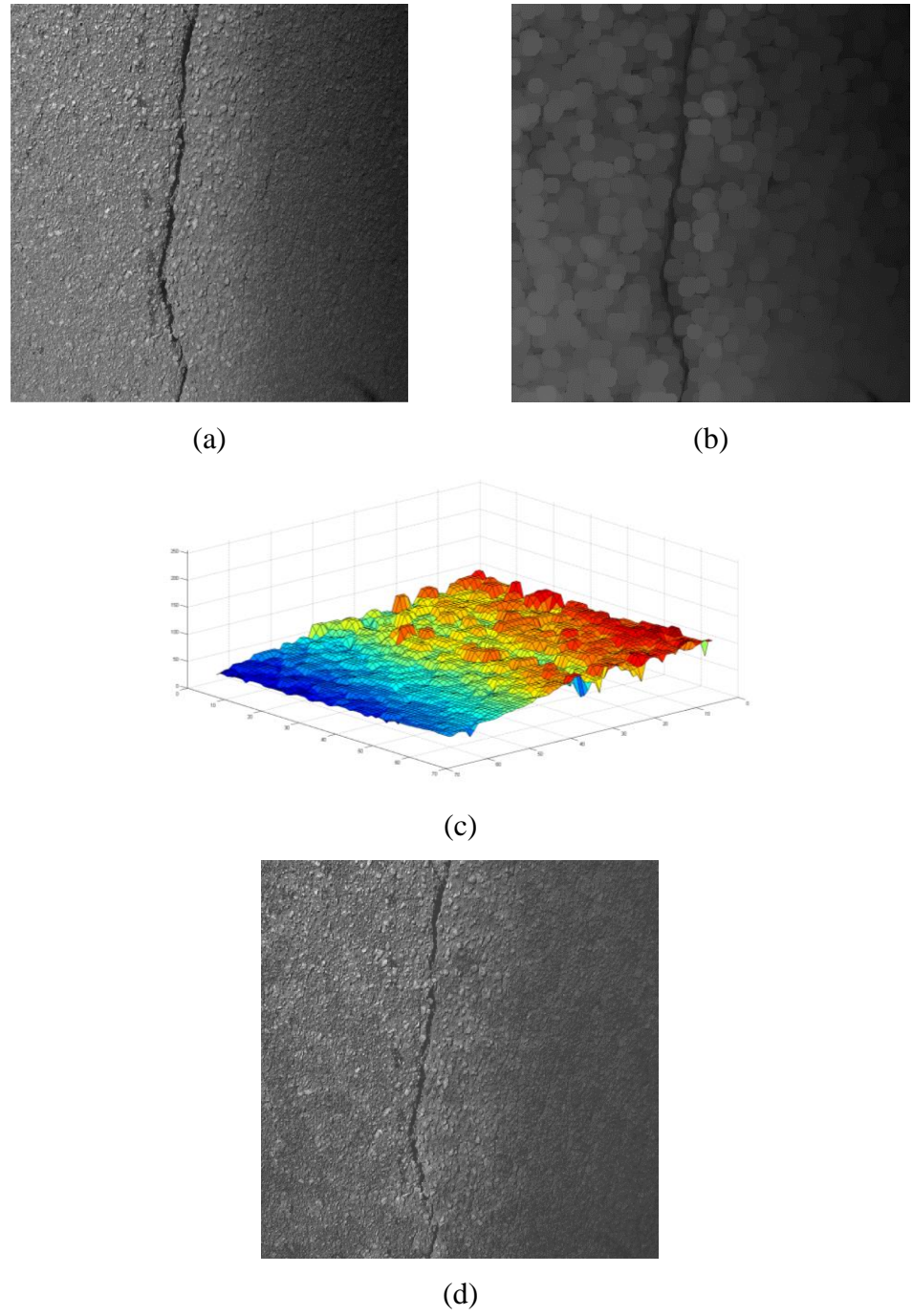


Figure 16 – Non-uniform Background Illumination Correction
 (a) Original Pavement Image With Non-uniform Illumination of Background
 (b) Non-uniform Illuminated Background Extracted By Morphological
 Opening Operation (c) Intensity Surface of the Background in 3D Space (d)
 Pavement Image After Removal of Non-uniform Illumination Effect

3.1.2. Wavelet Denoising

Even though the Fourier transform has been the pillar of transform-based image processing since the late 1950s, recently, wavelet transform has shined because of its easiness and effective compression techniques of the images. Instead of sinusoids used in Fourier transform, wavelet transforms are based on small waves with varying frequency and limited duration, called as wavelets (Gonzalez & Woods 2008).

Wavelets were first introduced as basis of a powerful approach to signal processing and analysis, named multiresolution theory outlined by Mallat (1989). This theory integrates and combines variety of disciplines such as audio processing, digital speech recognition and image processing. The approach was simple such that if features cannot be detected at one resolution, they may be easy to detect at another one. Examples of wavelet transform can be given ranging from image coding to edge detection and noise removal. Our aim in this section is to introduce its fundamentals within the context of image denoising using wavelets.

Wavelet denoising efforts focus on removing the noise in the signal while preserving the signal characteristics, regardless of its frequency content. A general procedure for denoising is as follows:

1. Linear forward wavelet transform
2. Nonlinear thresholding step
3. Linear inverse wavelet transform

The process is explained below in detail was introduced by Rangarajan et al. (2002).

Assume that the noisy signal $X(t)$ is represented by:

$$X(t) = S(t) + N(t) \quad (7)$$

where $S(t)$ is the raw signal and $N(t)$ is additive noise. Let $W(X)$ and $W^{-1}(Z)$ denote the forward and inverse wavelet operators, respectively and $D(x, \lambda)$ represent the denoising operator with threshold λ . It is aimed to denoise $X(t)$ to recover $\hat{S}(t)$ as an estimate of $S(t)$. The procedure can be summarized in three steps given in Equations (8) to (10):

$$Y = W(X) \quad (8)$$

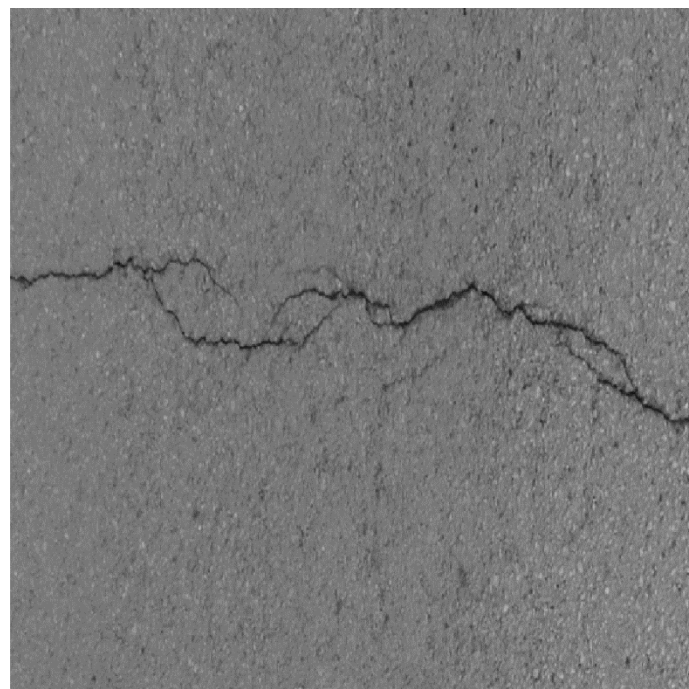
$$Z = D(Y, \lambda) \quad (9)$$

$$\hat{S} = W^{-1}(Z) \quad (10)$$

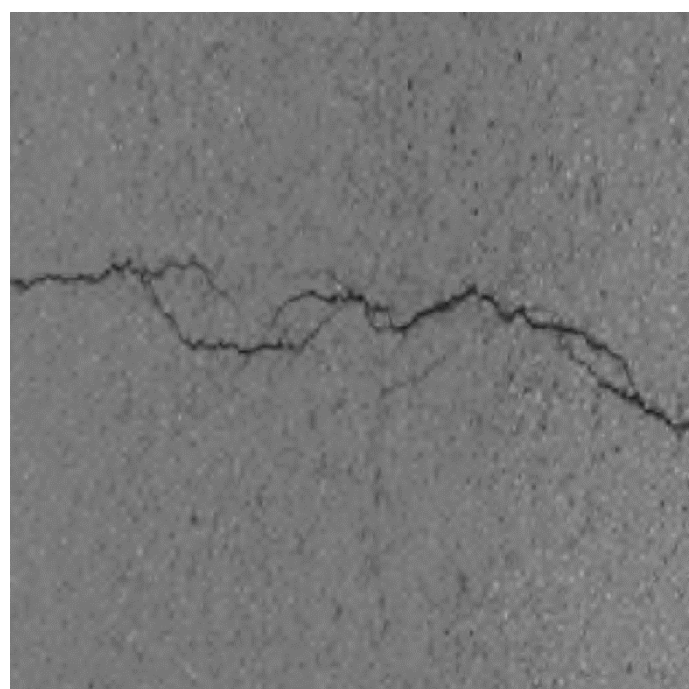
The soft thresholding operator which shrinks coefficients above the threshold value is defined as:

$$D(Y, \lambda) = \text{sgn}(Y) \max(0, |Y| - \lambda) \quad \text{or} \quad D(Y, \lambda) = \begin{cases} Y - \lambda & Y > \lambda \\ 0 & |Y| \leq \lambda \\ Y + \lambda & Y < -\lambda \end{cases} \quad (11)$$

Selection of threshold value λ is an important question for the effectiveness of the wavelet denoising procedure. A small threshold may not affect the input image, so the result may still be noisy. On the other hand, a large threshold produces a too much smoothed image where important parts of the image might be removed. An example result of the wavelet denoising is shown in Figure 17.



(a)



(b)

Figure 17 - Wavelet Denoising (a) Before Wavelet Denoising (b) After Wavelet Denoising

3.1.3. Local Thresholding based Image Segmentation

The majority of the algorithms are based on the assumption that crack pixels are darker than the surrounding pixels. Therefore, to eliminate background from the crack pixels, generally a global threshold is applied. Pixels with intensity values less than a certain threshold level are labeled as zero (crack pixels) and all pixels greater than threshold are labeled as one (non-crack pixels), given in Equation (12), where $g(x,y)$ represents the intensity value of the image,

$$g(x,y) = \begin{cases} 1 & \text{if } f(x,y) > \tau \\ 0 & \text{if } f(x,y) \leq \tau \end{cases} \quad (12)$$

and τ is a constant applicable over an entire image, the process given in this equation is referred to as global thresholding (Gonzalez & Woods 2008). In practice, it is hard to find a universal threshold value applicable for all images. Therefore, an appropriate threshold value has to be calculated for each pavement image using its own pixel intensity distribution.

In this study, two threshold values are calculated for each pavement image using different methods. The first threshold is obtained through the application of self-adaptive local thresholding method proposed by Salari and Bao (2010). In this method, each image is divided into a set of non-overlapping blocks and only the blocks including crack pixels are considered when calculating threshold (Figure 18b). Since crack blocks have lower average intensities and higher standard deviations compared to non-crack ones, average intensity and standard deviation parameters are used to distinguish the crack blocks including crack pixels from the non-crack ones. Once crack blocks are identified, Otsu (1979) algorithm is applied to each of these blocks and individual threshold values are obtained. Lastly, the average of these individual threshold values is selected to be the first threshold value for segmentation purposes. It should be kept in mind that the block size is critical when identifying crack blocks.

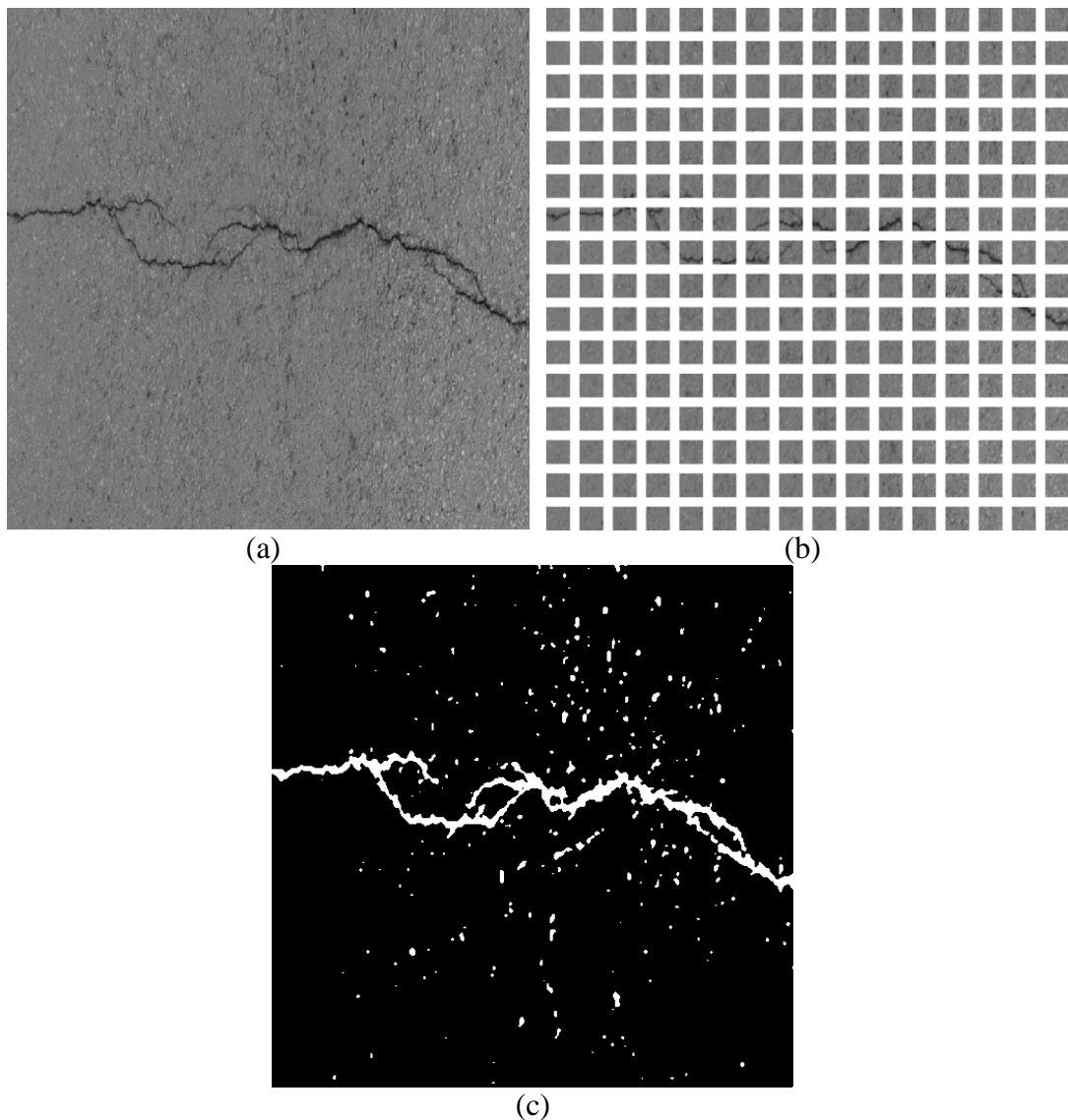


Figure 18 – Thresholding (a) Input Image (b) Subdivision of the Image into Non-Overlapping Blocks (c) Binary Image Obtained from Thresholding

It has to be large enough to include the crack and background pixels together. Thus, it is selected to be 32×32 rectangle box in this study. The second threshold value is calculated using Otsu's algorithm once again, but this time the image is taken into account as a whole rather than small blocks.

Having calculated the first and second threshold values, the smaller of these two is selected as the final threshold value. In this manner, low gray value noises could be

reduced effectively to prevent misclassification of the results. Finally, a binary image is obtained through classification of pixels with their corresponding intensities smaller than the final threshold value as crack candidates, and the others as background (Figure 18c).

3.1.4. Post Processing and Image Enhancement

Post processing is the last step for the detection of crack candidates. The purpose is to purify the crack candidate regions from the noise and to enhance the structure of the cracks. To accomplish this, threshold applied pavements images are passed to a median filter and then, noise cancellation and morphological closing operations are applied consequently.

3.1.4.1. Median Filtering

Median filter is the one of best-known non-linear filtering operation in digital image processing. As its name implies, each pixel is replaced with the median of the neighborhood pixels. Median filters are very popular, as they provide superior noise reduction capabilities compared to linear smoothing filters of similar size. Salt and pepper noise included images can be purged by applying median filter. While it is removing the noise effectively, it preserves most of the boundaries and useful details in the image (Richards 2013).

In order to accomplish median filtering at a point in an image, first, the values of the pixel in the neighborhood are sorted and their median is determined. This value is then assigned to the corresponding pixel in the filtered image. For example, assume that a 3×3 neighborhood has values (153, 148, 130, 129, 117, 102, 250, 246, 245). These values are sorted as (102, 117, 129, 130, 148, 153, 246, 245, 250) in an increasing

order, which results in a median of 148. Thus, the center value is replaced by the median of all nine values as shown in Figure 19.

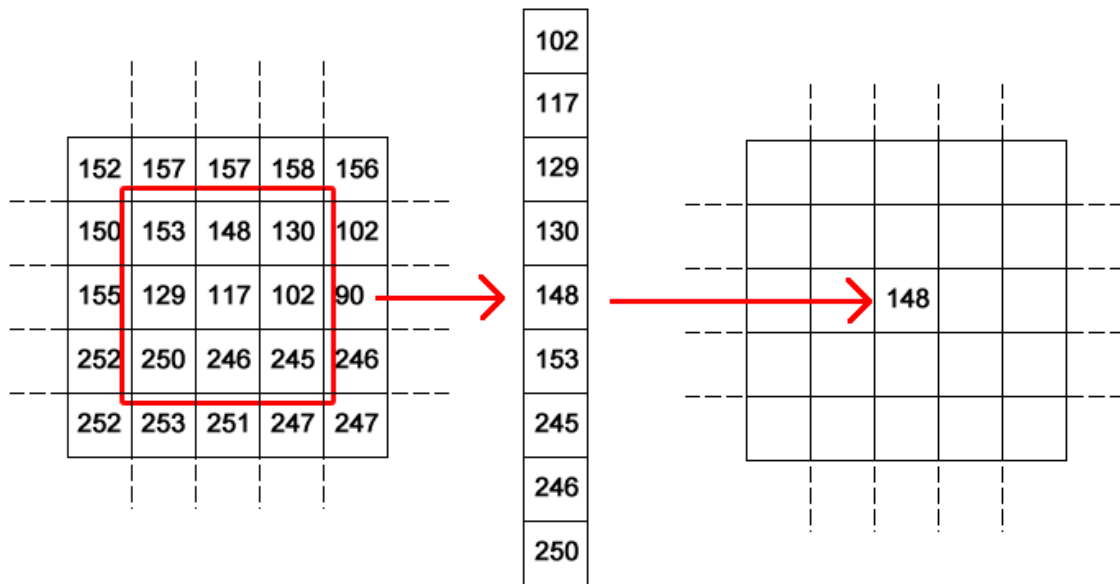
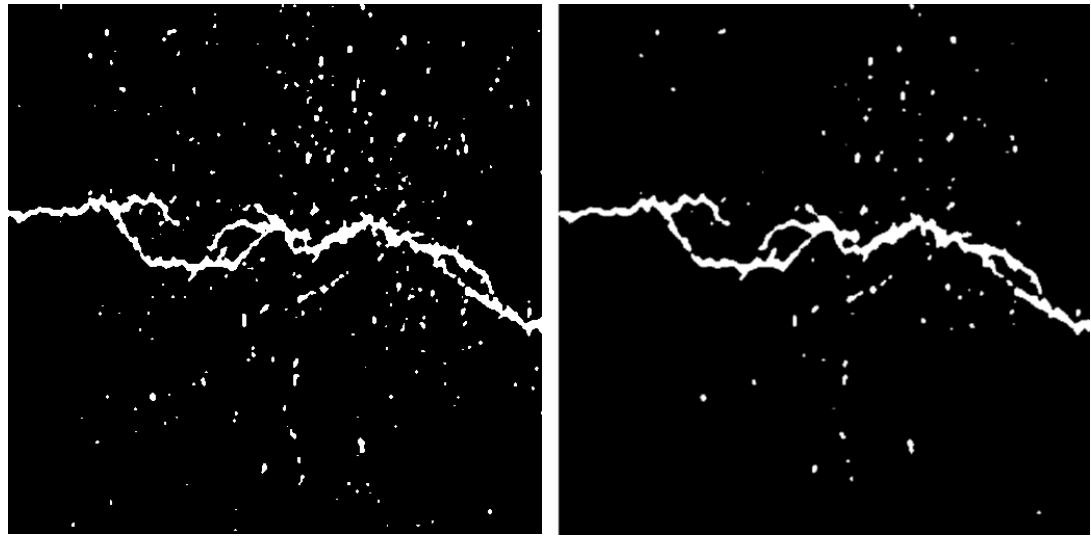


Figure 19 - An Example of Median Filtering

In the proposed method, a rectangle element of 3×3 pixels is designed and median filtering is performed in binary images to remove small noisy regions. The result of this operation is illustrated in Figure 20.



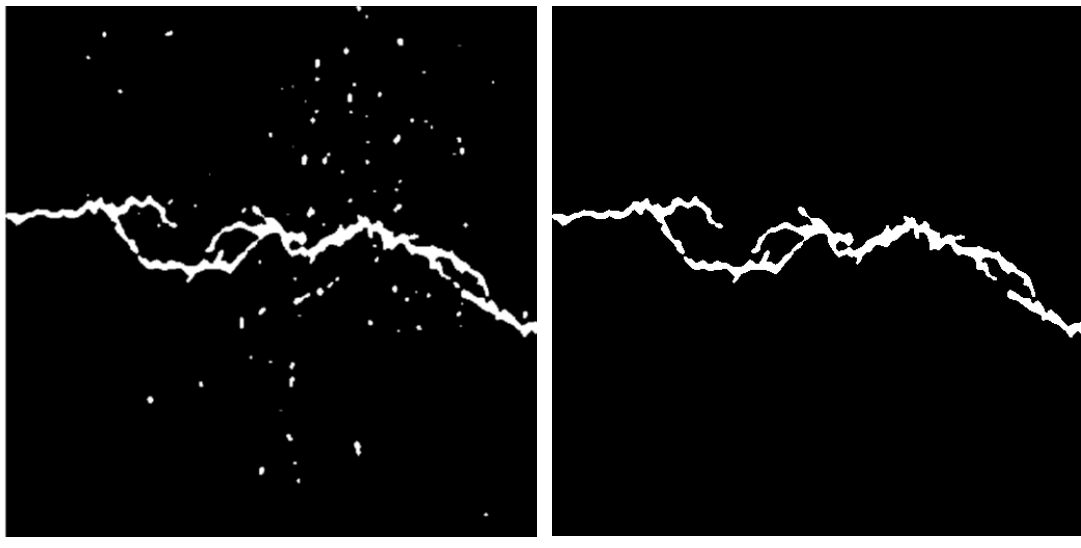
(a)

(b)

Figure 20 - Median Filtering (a) Before (b) After

3.1.4.2. Noise Cancellation

Dark regions rather than crack pixels in the original image may still remain after applying the median filter. These regions may come from oil stains and tire marks, which are relatively smaller than the crack regions. Therefore, minor connected components whose areas are under a preset value are removed. According to the experiments performed with the images, this value is chosen to be 500 pixels based on the experience. At the end, most of the noise is cleaned from the binary image. The resultant image is shown in Figure 21.



(a) (b)

Figure 21 - Noise Removal (a) Before (b) After

3.1.4.3. Morphological Closing Operation

Previous steps may break the connected components of pavement image and produce small gaps among them. Although they are obtained from the same parent crack, new connected components may arise and can be treated as new cracks. To solve this ambiguity, a set of morphological operators is applied on an image.

By definition, morphological operation is a template based processing, generally defined in terms of a structuring element (SE) of any shape or size as discussed in the previous sections. For any location in an image, the result of applying the structuring element is a decision about whether the pixel under the center of the SE is a member of the object or not. Morphological operations are generally applied for binary images, having less regular boundaries due to system noise. Most of these operations are based on simple expanding and shrinking operations. Basic morphological operations are dilation and erosion, the details of which are explained below:

If any part of SE is outside the object, i.e., crack body, the center pixel of SE is removed from the object, which is called erosion. Consequently, erosion has the effect of

eroding and reducing the size of an object. The main advantage of using erosion is that it can help reducing the irregular edges. Erosion can be expressed as:

$$E = O \ominus S \quad (13)$$

Where S represents the structuring element and O represent the binary image. E is the set of pixels that describes the eroded object. The symbol \ominus is used to represent erosion. Figure 22 shows the effect of eroding the objects with a square SE of size 3 x 3. As seen, the result is a greatly reduced object. In this case, the holes and gaps between different regions becomes larger, and small details are eliminated.

Dilation is the opposite of erosion operation. If SE partly overlaps the object, i.e., crack body, the inclusion decision about the center pixel of SE is part of an object is simply dilation. This operation grows the size of the object and fills the holes. Its notation is the same as above except calling the set of pixels that describe the dilated object D according to Equation (14).

$$D = O \oplus S \quad (14)$$

where the symbol \oplus is used to denote dilation. Figure 23 shows the effect of dilation operation on the object with a square SE of size 3 x 3. In this figure, small holes are enclosed and objects are significantly expanded.

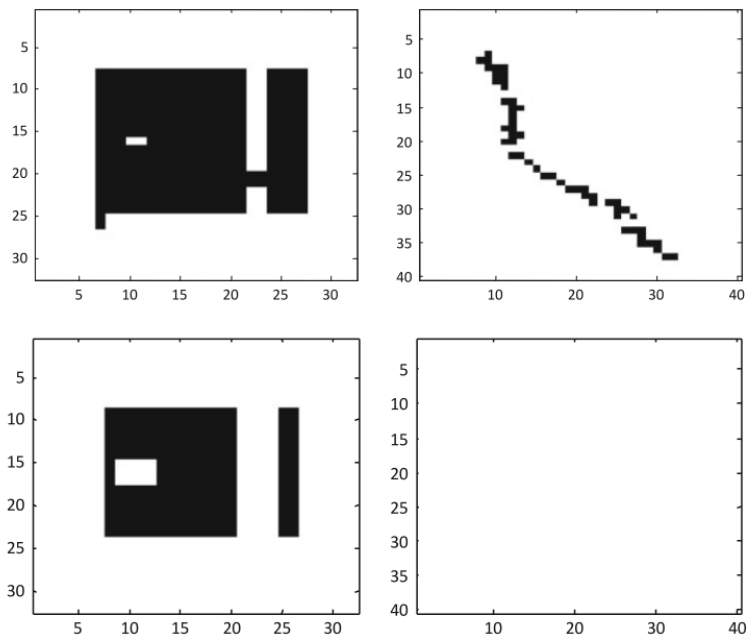


Figure 22 - Erosion of the Object Using 3×3 Structuring Element (Richards 2013)

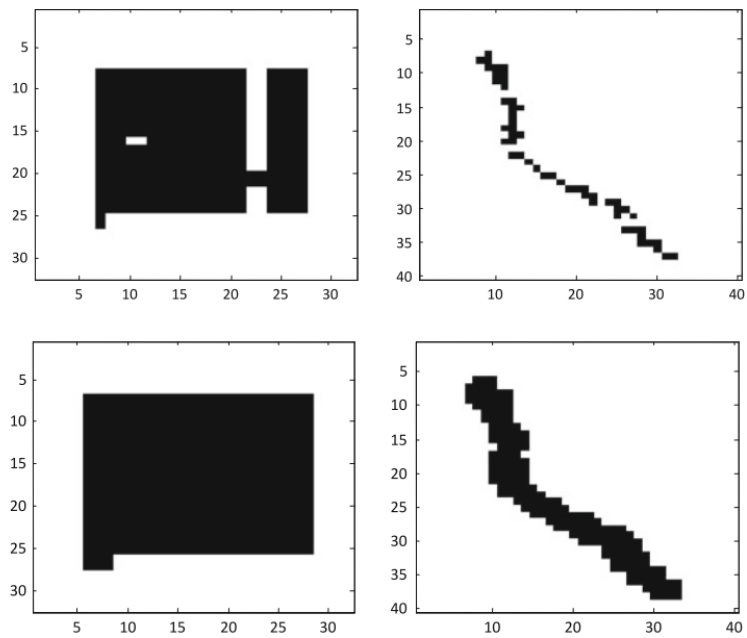


Figure 23 - Dilation of the Object Using 3×3 Structuring Element (Richards 2013)

Erosion and dilation are dual operations in that they have inverse effects. However, the sequential application of erosion and dilation or vice versa, give valuable results. Erosion followed by dilation is referred to as opening (denoted by \circ), given in Equation (15):

$$P = O \circ S = (O \ominus S) \oplus S \quad (15)$$

On the other hand, dilation followed by erosion is called closing (denoted by \bullet), given in Equation (16):

$$C = O \bullet S = (O \oplus S) \ominus S \quad (16)$$

The terms “opening” and “closing” are meaningful as seen from the results of their application. The term “opening” is used because it can open up a gap between the objects connected by a thin bridge of pixels. Any regions that survive the erosion are restored to their original size by the dilation (Figure 24). In the same manner, “closing” is used because the operation can fill holes in the regions while preserving the initial region sizes (Figure 25).

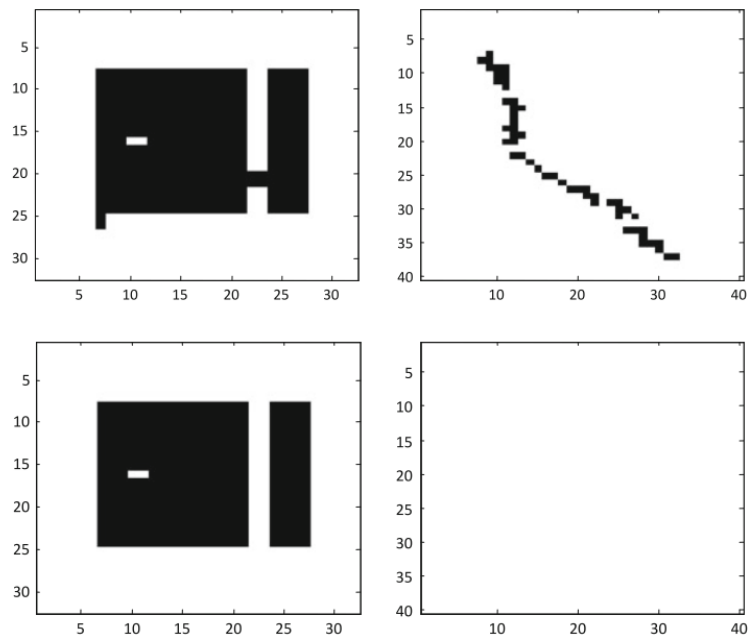


Figure 24 - Result of Applying Opening Operation (Richards 2013)

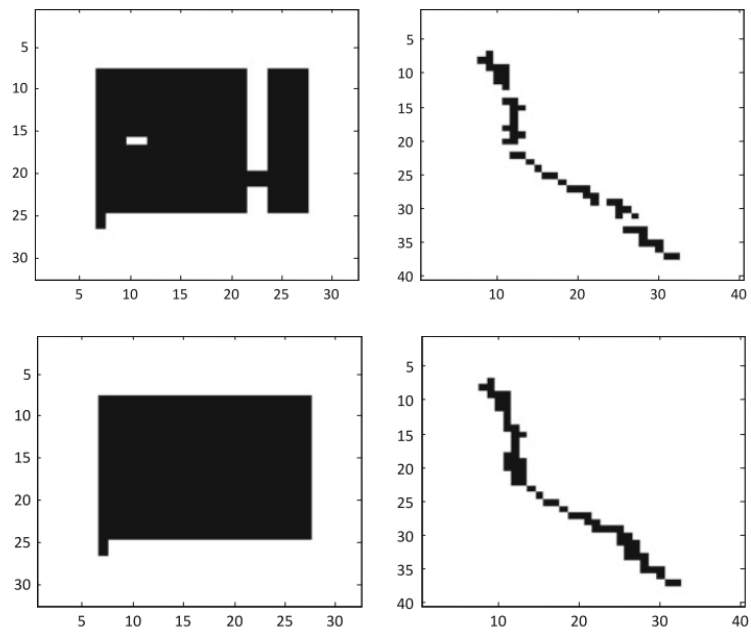


Figure 25 - Result of Applying Closing Operation (Richards 2013)

In the proposed method, closing operation is implemented. A diamond shape of 5 pixel radius structuring element is used to perform for this morphological operation (Figure 26). As a result, small openings are closed and nearby crack candidates are merged without changing the shape of the connected components (Figure 27).

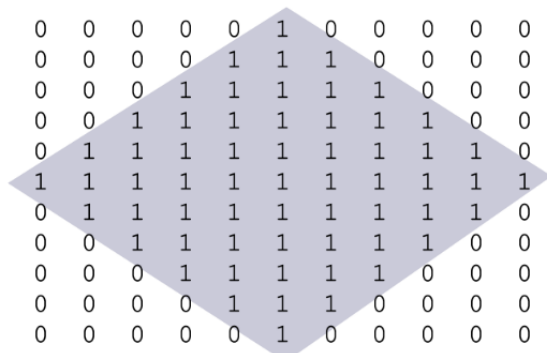


Figure 26 - Diamond Shape Structuring Element with 5 Pixels Radius

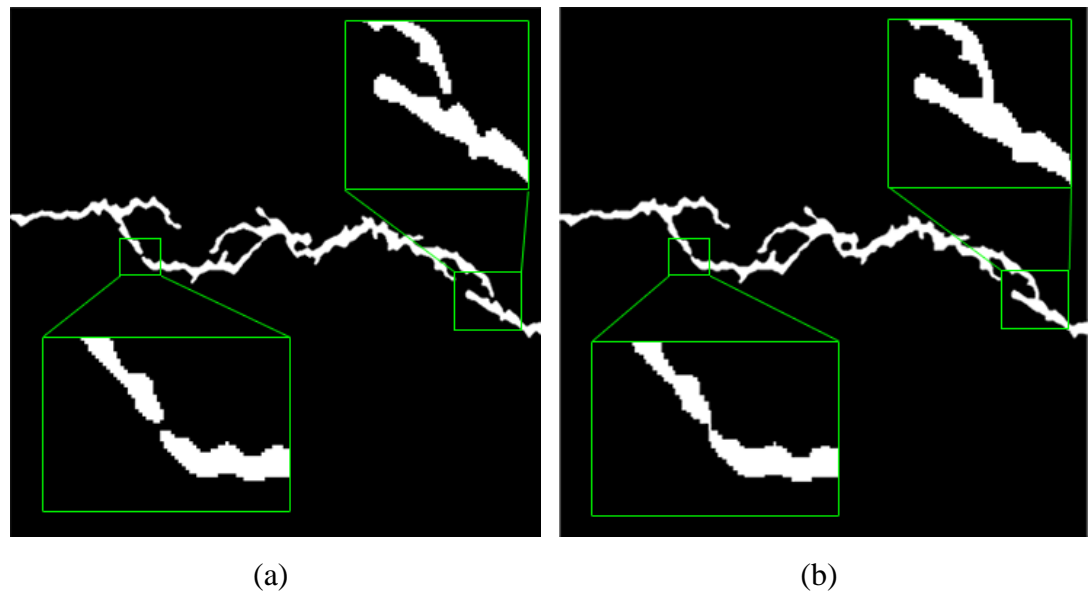


Figure 27 - Morphological Closing Operation Illustration (a) Before (b) After

3.2. Crack Classification

In the previous part, crack and non-crack regions are extracted from the background and prepared for classification purposes. Consequently, a machine learning based pavement crack classification procedure is followed in this part. First, to teach the computer “what is crack” and “what is not”, cracks are defined using their geometric features. Then a SVM model is trained with these properties. Last, unknown crack candidate regions are tested and labeled using the SVM model.

3.2.1. Feature Extraction

Crack candidate regions enhanced from the previous steps are aimed to be categorized into four different classes of cracks: transverse, longitudinal, alligator, and non-crack. Since these types differ from each other considering their shapes, their geometric properties can be used to classify them into different classes. For example, longitudinal and transverse cracks are thin and long shapes, however, they have distinct orientations. Meanwhile, alligator cracks and non-cracks cover large areas compared to longitudinal and transverse cracks. In addition, non-crack regions deviate from the cracks because they are filled with more white pixels than regular cracks. Therefore, various geometric parameters can be defined to group them mathematically. For this purpose, following features are defined for crack identification (Gungor & Pekcan 2013). Table 1 provides the typical values of these features.

1. *Extent (E)*: Ratio of bounding rectangle’s area that encloses the region to the area of region itself. (Figure 28b) It takes values between 0 and 1. The definition of extent is given in Equation (17);

$$E = \frac{A_b}{A} \quad (17)$$

where

A_b : the area of bounding rectangle that encloses the region

A : the area of the region

2. *Aspect Ratio (AR)*: It is ratio of distance between the leftmost and rightmost point to distance between the upmost point and lowermost point. It is simply illustrated in (Figure 28c). The definition of aspect ratio is given in Equation (18):

$$AR = \frac{w}{h} \quad (18)$$

where

w : distance between the leftmost and rightmost point

h : distance between the upmost point and lowermost point

3. *Label (l)*: If AR is higher than 2 then the region is labeled 1. If $1/AR$ is greater than 2, it is labeled -1 and 0 otherwise.
4. *Orientation (θ)*: It provides the angle between the horizontal axis and major axis of the representative ellipse. The value is in degrees, ranging from 0 to 90. Figure 28e illustrates the axes and orientation of the ellipse, where the orientation is the angle between the horizontal dotted line and the major axis.
5. *Eccentricity (ε)*: The eccentricity is calculated by dividing the distance between two focus point to the length of its major axis (Figure 28f). It can be

thought of as a measure of how much the ellipse deviates from being a circle. The definition of eccentricity is given in Equation (19);

$$\varepsilon = \frac{d_f}{d_m} \quad (19)$$

where

d_f : distance between two focus point

d_m : the length of major axis

6. *Circularity Ratio (R_c)*: It is computed using the formula below. The value of this measure is 1 for a circular region and $\pi/4$ for a square. Circularity ratio is a dimensionless measure and thus, insensitive to uniform scale changes; it is insensitive also to orientation. The definition of circularity ratio is given in Equation (20);

$$R_c = \frac{4\pi A}{P} \quad (20)$$

where

A : the area of the region

P : the perimeter of the region

7. *Filling Index (F)*: It is defined to create an isolation between crack types, the definition of which is given in Equation (21):

$$F = \frac{P_{L_1} P_{L_2}}{L_1 L_2} \quad (21)$$

where

P_{L_1} : number of white pixels on the first diagonal

P_{L_2} : number of white pixels on the second diagonal

L_1 : lengths of first diagonal crossing the region

L_2 : lengths of second diagonal crossing the region

8. *Entropy (S)*: Image entropy is a quantity of the amount of the information stored in an image. Entropy is a measure of variability and is 0 for a constant image. Entropy of a region is calculated using Equation (22):

$$S = - \sum_{k=0}^{L-1} p_k \log(p_k) \quad (22)$$

where

L : number of gray values

p_k : probability associated with gray level k

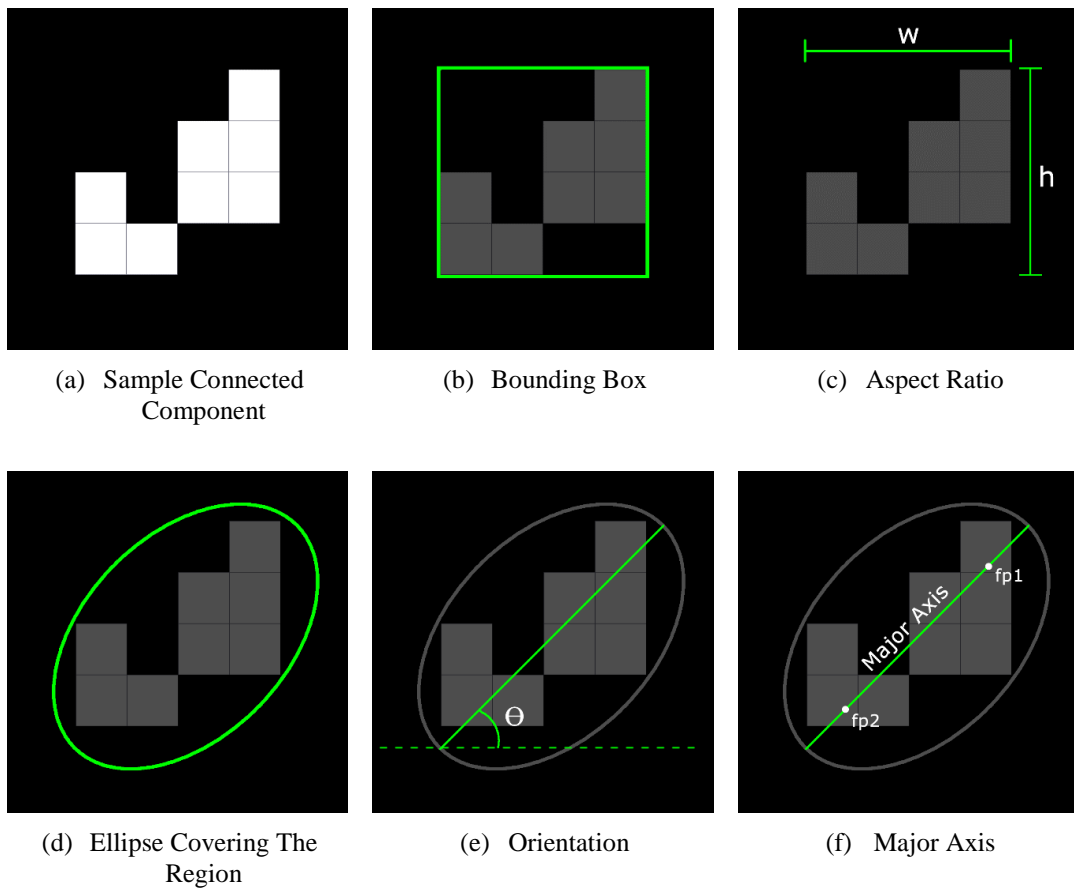


Figure 28 – Visualization of Geometric Features (Gungor & Pekcan 2013)

Table 1 - Typical Connected Component Feature Values

Region Type	Extent	Aspect Ratio	Label	Orientation	Eccentricity	Circularity Ratio	Filling Index	Entropy
Transverse	0.1100	3.9293	1	10.97	0.9833	0.0176	0.0657	0.5000
Longitudinal	0.1914	0.0920	-1	89.77	0.9979	0.0220	0.2055	0.7044
Alligator	0.2858	0.5695	0	59.29	0.8622	0.0084	0.2160	0.8632
Non-crack	0.6922	0.5238	0	47.05	0.8920	0.5863	0.9905	0.8906

3.2.2. Classification of Crack Types based on SVM

The Support Vector Machine (SVM) is a supervised learning method, originally introduced by Vladimir N. Vapnik and Alexey Ya. Chervonenkis in 1963. At first, SVMs went largely unnoticed due to a widespread belief in machine learning that they are neither suitable nor relevant for practical applications. In 1992, Bernhard E. Boser, Isabelle M. Guyon and Vladimir N. Vapnik suggested a modern way to create nonlinear classifiers by applying the kernel trick to maximum-margin hyperplanes (Boser et al. 1992). Since then, with their proven performance, SVMs have been extensively used in numerous real-world applications, such as bioinformatics, text mining, face recognition, and image processing. What makes SVMs so special is that they operate well in high number of dimensions and they are generally fast to compute.

SVM is used in the proposed method for classification of crack candidates. The main idea of SVM is constructing a linear decision boundary that separates the classes into two parts. The “best” hyperplane would be approximately equidistant between the borders of each of the two classes (Figure 29). Therefore, it is chosen according to the maximum margin principle that splits the data points by maximizing the perpendicular distance to the plane. Closest data points are called Support Vectors and this concept shapes the origin of the Support Vector Machines.

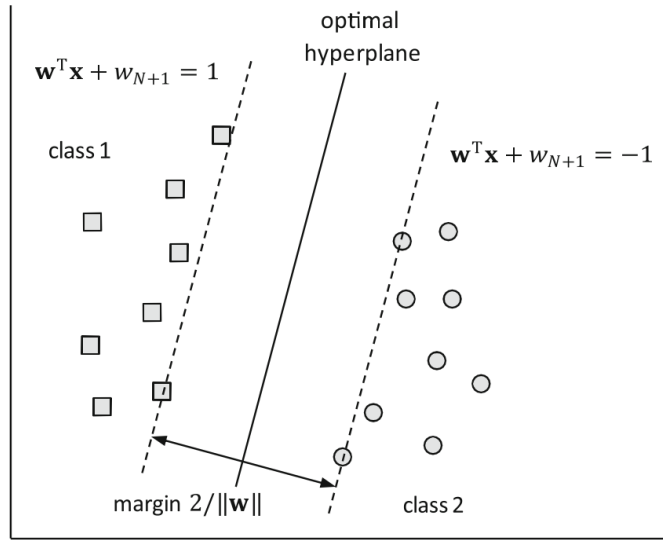


Figure 29 - An Optimal Separating Hyperplane (Richards 2013)

3.2.2.1. SVM Theory

Let's assume that, we have a linearly separable data that we can draw a line on a graph to separate them into two classes as class 1 and class 2 (Figure 29). The line or so called hyperplane can be formulated by:

$$f(\mathbf{x}) = \mathbf{w}^T \mathbf{x} + w_{N+1} = 0 \quad (23)$$

where \mathbf{w} is the normal vector to the hyperplane or weight vector, \mathbf{x} is the training data and w_{N+1} is the offset. The objective of SVM is to find an optimal hyperplane which is in the middle of two marginal hyperplanes touching the nearest pixels.

Referring to Figure 29, the equation of marginal hyperplanes;

$$\text{for class 1 pixels } \mathbf{w}^T \mathbf{x} + w_{N+1} = 1 \quad (24)$$

$$\text{for class 2 pixels } \mathbf{w}^T \mathbf{x} + w_{N+1} = -1 \quad (25)$$

The difference of perpendicular distances of these hyperplanes from the origin is defined as:

$$\text{margin} = \frac{|1 - w_{N+1}|}{\|\mathbf{w}\|} - \frac{|-1 - w_{N+1}|}{\|\mathbf{w}\|} = \frac{2}{\|\mathbf{w}\|} \quad (26)$$

The best position of an optimum separating hyperplane is found when the margin in Equation (26) is the largest. This happens when the weight vector $\|\mathbf{w}\|$ is smallest. This provides an aim for optimal training of the linear classifier. However, it should be ensured that every pixel vector stays on its correct side of the separating hyperplane, which defines a set of constraints that must be considered when finding the optimal hyperplane. Those constraints can be described mathematically in the following manner:

$$\begin{aligned} \text{for pixel } \mathbf{x}_i \text{ in its correct class } & y_i(\mathbf{w}^T \mathbf{x}_i + w_{N+1}) \geq 1 \\ \text{or } & y_i(\mathbf{w}^T \mathbf{x}_i + w_{N+1}) - 1 \geq 0 \end{aligned} \quad (27)$$

where y_i is an auxiliary variable which is equal to 1 for class 1, and -1 for class 2.

Minimizing $\|\mathbf{w}\|$ is equivalent to minimizing $\frac{1}{2} \|\mathbf{w}\|^2$ and the use of this term makes it possible to perform a standard quadratic optimization problem. The problem formulation is given in Equation (28):

$$\min \frac{1}{2} \|\mathbf{w}\|^2 \quad \text{such that} \quad y_i(\mathbf{w}^T \mathbf{x}_i + w_{N+1}) - 1 \geq 0 \quad (28)$$

Constrained minimization can be handled by the process of Lagrange multipliers. Therefore, the Lagrangian function for SVM is constructed by augmenting the objective function with a weighted sum of the constraints:

$$L_p = \frac{1}{2} \|\mathbf{w}\|^2 - \sum_i a_i \{y_i(\mathbf{w}^T \mathbf{x}_i + w_{N+1}) - 1\} \quad (29)$$

where a_i are called Lagrange multipliers and positive by definition.

The L_p should be minimized with respect to \mathbf{w} , w_{N+1} and maximized with respect to $a_i \geq 0$. It can be done by equating the derivatives of L_p with respect to the weights (\mathbf{w} and w_{N+1}) to zero. Noting that: $\|\mathbf{w}\|^2 = \mathbf{w}^T \mathbf{w}$

$$\frac{\partial L_p}{\partial \mathbf{w}} = \mathbf{w} - \sum_i a_i y_i \mathbf{x}_i = 0 \quad (30)$$

which gives

$$\mathbf{w} = \sum_i a_i y_i \mathbf{x}_i \quad (31)$$

and

$$\frac{\partial L}{\partial w_{N+1}} = - \sum_i a_i y_i = 0 \quad (32)$$

Equation (31) and Equation (32) can be substituted in Equation (29). However, before that, operation below should be performed first:

$$\| \mathbf{w} \|^2 = \mathbf{w}^T \mathbf{w} = \sum_j a_j y_j \mathbf{x}_j^T \sum_i a_i y_i \mathbf{x}_i \quad (33)$$

Substituting the above ones into Equation (29) gives:

$$L_D = \frac{1}{2} \sum_j a_j y_j \mathbf{x}_j^T \sum_i a_i y_i \mathbf{x}_i - \sum_i a_i \left\{ y_i \left(\sum_i a_i y_i \mathbf{x}_i^T \mathbf{x}_i + w_{N+1} \right) - 1 \right\}$$

i.e. $L_D = \frac{1}{2} \sum_{i,j} a_i a_j y_i y_j \mathbf{x}_j^T \mathbf{x}_i - \sum_{i,j} a_i a_j y_i y_j \mathbf{x}_j^T \mathbf{x}_i - w_{N+1} \sum_i a_i y_i + \sum_i a_i$

Using Equation (32) this simplifies to

$$L_D = \sum_i a_i - \frac{1}{2} \sum_{i,j} a_i a_j y_i y_j \mathbf{x}_j^T \mathbf{x}_i \quad (35)$$

Equation (35) gives a new formulation which is dependent on a_i and needs to be maximized according to Equations (32), (33), and (34):

$$L_D = \sum_i a_i - \frac{1}{2} \sum_{i,j} a_i a_j y_i y_j \mathbf{x}_j^T \mathbf{x}_i \quad s.t. \quad a_i \geq 0 \quad \forall i, \quad \sum_{i,j} a_i y_i = 0 \quad (36)$$

$$L_D = \sum_i a_i - \frac{1}{2} \sum_{i,j} a_i H_{ij} a_j \quad \text{where } H_{ij} = y_i y_j \mathbf{x}_j^T \mathbf{x}_i \quad (37)$$

$$L_D = \sum_i a_i - \frac{1}{2} \mathbf{a}^T \mathbf{H} \mathbf{a} \quad \text{s.t. } a_i \geq 0 \forall i, \quad \sum_i a_i y_i = 0 \quad (38)$$

If \mathbf{w} is known, all a_i values can be found, on the other hand, if all a_i values are known, \mathbf{w} can be calculated. This new formulation L_D is called as *Dual form* of the *Primary* L_p . It should be noted that Dual form requires only the dot product of each input vector of \mathbf{x}_i to be calculated. This is worthy for *Kernel Trick* which will be explained in the following paragraphs.

As a result, the problem is modified to minimizing L_p instead of maximizing L_D as given in Equation (35):

$$\max_a \left[\sum_i a_i - \frac{1}{2} \mathbf{a}^T \mathbf{H} \mathbf{a} \right] \quad \text{s.t. } a_i \geq 0 \forall i, \quad \sum_{i,j} a_i y_i = 0 \quad (39)$$

The above problem is a convex quadratic optimization problem that should be solved by a QP solver which will give \mathbf{a} . So \mathbf{w} can be calculated from Equation (31). So the only remaining unknown is w_{N+1} .

Any Support Vector which satisfies Equation (32) has this form:

$$y_s (\mathbf{w}^T \mathbf{x}_s + w_{N+1}) - 1 = 0 \quad (40)$$

Substituting Equation (31) in Equation (40) yields Equation (41):

$$y_s \left(\sum_{k \in S} a_k y_k \mathbf{x}_m^T \mathbf{x}_s + w_{N+1} \right) - 1 = 0 \text{ or} \quad (41)$$

$$y_s \left(\sum_{k \in S} a_k y_k \mathbf{x}_m^T \mathbf{x}_s + w_{N+1} \right) = 1$$

where s indicates the set of indices of the Support Vectors. It can be defined by finding the indices i where $a_i \geq 0$. Multiply both sides with y_s remembering $y_s^2 = 1$:

$$y_s^2 \left(\sum_{k \in S} a_k y_k \mathbf{x}_m^T \mathbf{x}_s + w_{N+1} \right) = y_s \quad (42)$$

$$w_{N+1} = y_s - \sum_{k \in S} a_k y_k \mathbf{x}_m^T \mathbf{x}_s \quad (43)$$

At the end of the process, we have the variables \mathbf{w} and w_{N+1} that define optimal separating hyperplane orientation and so the required Support Vector Machines.

The above procedure is valid only for linearly separable cases. However, most data are not linear and have many dimensions. If the problem is nonlinear, the data can be mapped to a new corresponding space by doing a nonlinear transformation using basis functions. Then the data become linearly separable in the higher order space (Figure 30). This transformation is called as kernel trick.

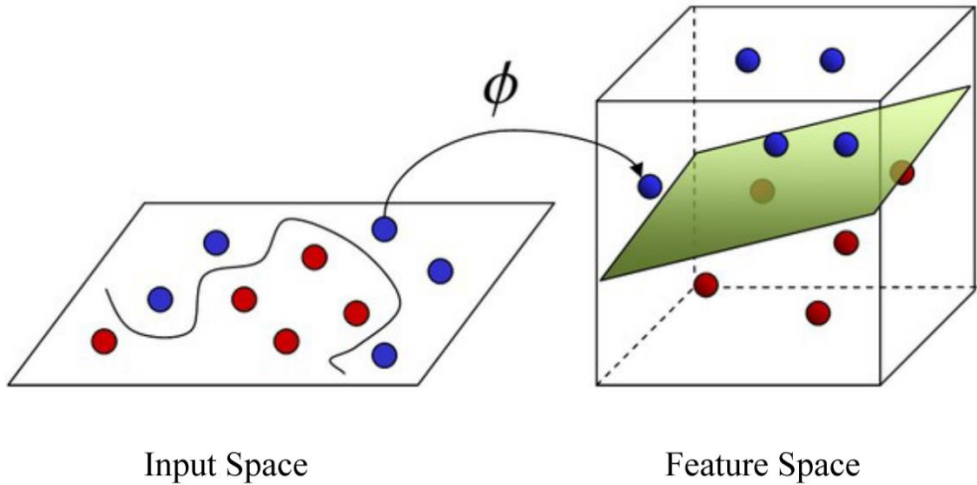


Figure 30 - Non-Linear Mapping: The 2D Input Space is Projected on 3D Space

For linearly separable case, a matrix H is defined from the dot product of input variables:

$$H_{ij} = y_i y_j \mathbf{x}_j^T \mathbf{x}_i = y_i y_j k(\mathbf{x}_i, \mathbf{x}_j) \quad (44)$$

In the above equation, we called $k(\mathbf{x}_i, \mathbf{x}_j)$ as a *Kernel Function* which is being known as a Linear Kernel ($k(\mathbf{x}_i, \mathbf{x}_j) = \mathbf{x}_j^T \mathbf{x}_i$). Kernel function is composed of variations of inner products of two vectors. That means the data can be transformed into a higher dimensionality space by non-linear feature mapping functions $\mathbf{x} \rightarrow \phi(\mathbf{x})$. The actual transformation of $\phi(\mathbf{x})$ does not need to be known because training data entering the calculation are in the product form. There are three common kernels defined as:

- Polynomial:
$$k(\mathbf{x}_i, \mathbf{x}_j) = [\mathbf{x}_j^T \mathbf{x}_i + a]^b$$

- Radial Basis Function: $k(\mathbf{x}_i, \mathbf{x}_j) = e^{-a\|\mathbf{x}_i - \mathbf{x}_j\|^2}$
- Sigmoid: $k(\mathbf{x}_i, \mathbf{x}_j) = \tanh(a\mathbf{x}_j^T \mathbf{x}_i - b)$

where a and b are parameters defining the kernel's behavior. Those kernels transform linearly not separable classes into separable ones in an efficient way.

In this study, since dimension of feature vector is greater than 2, it is not possible to illustrate the data to look at whether it is linearly separable or not. Because of that, kernel trick is used to map input space to a higher dimensional space as mentioned above. As a kernel function radial basis function is implemented in this study. The parameters of the kernel are calculated by three-fold cross validation. Details of implementation of SVM and its results are discussed in Chapter 4.

3.2.2.2. Multi-Class SVM

Since the Support Vector classifier assigns unknown data points into one of just two classes, a strategy is needed to allow its use in the multi-class situations. Researchers developed many approaches to address the multi-classification problem. One against one and one against all are the two popular examples of multi-class approaches. In this study, one-against-all approach is implemented with four classifiers for each crack type including the non-crack one. It is one of the earliest and most commonly used multiclass SVMs which constructs a number of binary SVM classifiers with the same number of classes. Each classifier differentiates one class from all the others. In other words, one against all method assigns a data point to a specific class if and only if that class has admitted it, while other classes have not, which leaves undecided regions in the feature space when more than one class accepts it or when all classes reject it (Awad & Khanna 2015).

CHAPTER 4

FIELD EXPERIMENTS

In this chapter, the proposed pavement crack identification system including the image processing methods are validated using real pavement crack images. For the purpose of performance verification, several experiments were performed in Middle East Technical University (METU) campus. Pavement photos including crack and non-crack regions were taken from different areas of campus roads, as shown in Figure 31. In this figure, the blue points indicate the points where the experiments were performed and the images were taken.

During the experiments, a quadcopter called DJI Inspire 1 was operated as shown in Figure 32. This UAV weighs around 3 kilograms when battery and camera are included. Its camera has 12.4 MP sensor and 20 mm focal length with the capability of recording 4K videos at 30 fps and 1080p videos at 60 fps. The camera is equipped with a rectilinear curved lens that provides 94° wide-angle field of vision without distortion. The system also comes with a 3-axis gimbal. With a single battery, it has an approximate flight time of around 20 minutes. The device is also equipped with a vision positioning and a sonar system. More technical specifications are also given in Table 2.

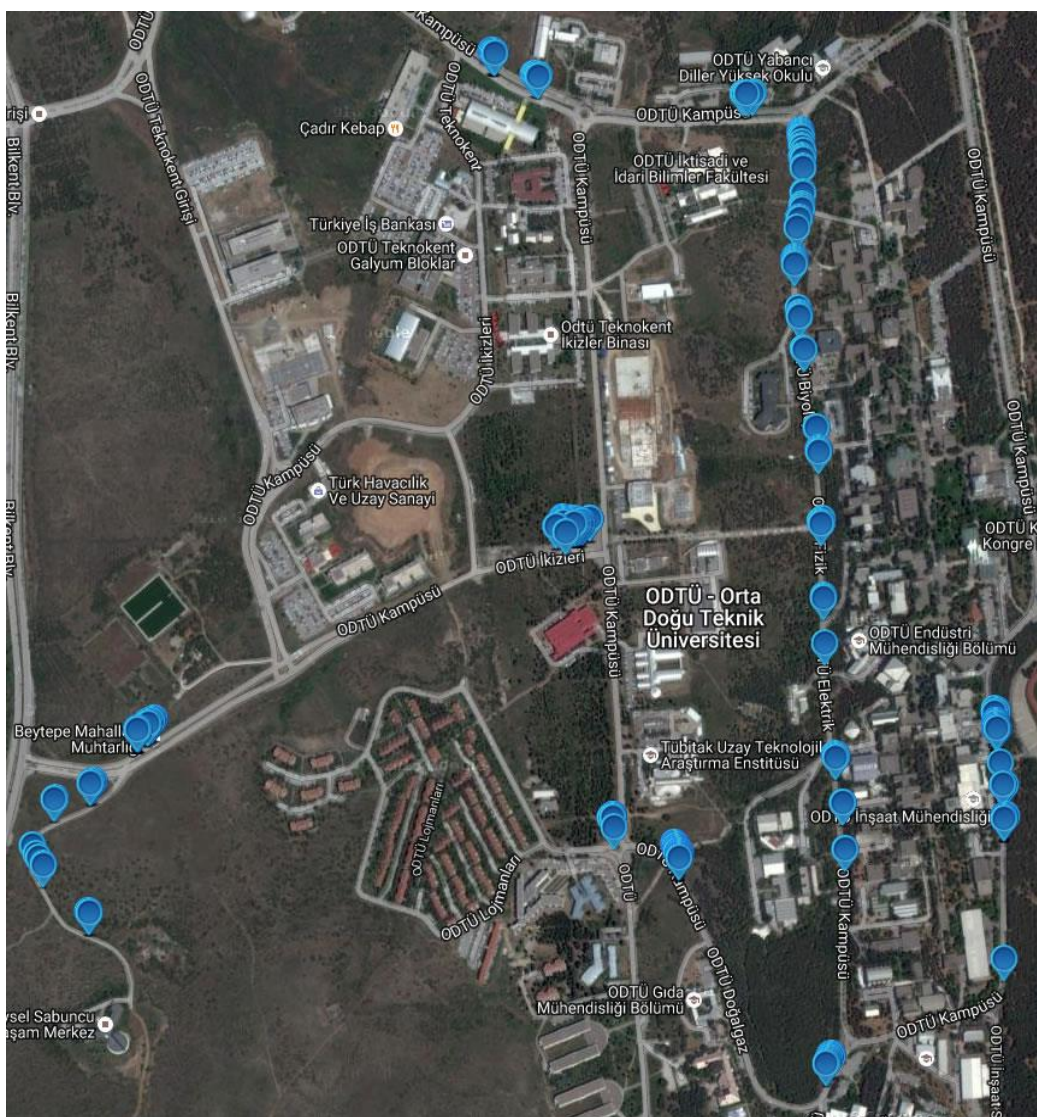


Figure 31 - Image Locations on Middle East Technical University Campus



Figure 32 - DJI Inspire 1 Quadcopter

Table 2 - Specifications of DJI Inspire 1 Used in the Experiments (DJI 2016)

Supported Battery	LiPo 6S High voltage battery
Weight (Battery & Propellers Included)	2935 g
Max Flight Time	Approximately 20 minutes
Max Flight Speed	22 m/s
Indoor Hovering	Enabled by default
Diagonal Length	559 to 581 mm
3-axis Camera Stabilization Gimbal	Yes
Gimbal Controllable Range	Pitch: -90° to +30°, Pan: ±320°
Camera Effective Pixels	12.4Megapixels
Camera Resolution	4000x3000
HD Recording	4096x2160p24/25, 3840x2160p24/25/30
Camera Recording FOV	94°
Communication Distance (Open Area)	2 km

Throughout the pavement crack finding studies, UAV flights were performed by camera looking at one lane only. Speed bumps and road markings were not considered when taking photos since detecting such features are not in the scope of this study. In order not to have shadows of UAV on the images, the image data were collected in the early morning hours or in the afternoon.

Pavement images were taken at different altitudes ranging from 0.5 m to 3 m. UAV's camera was facing directly towards the surface of the pavement. Using the quadcopter, total of 261 pavement images were taken along the roads of METU campus during daylight conditions. Data were stored in a micro SD card embedded into UAV. Using those images, the crack candidate detection and crack classification process were utilized offline, i.e., the pictures were transferred to a personal computer after the flight.

The data set consists of RGB color images with 4000 x 3000 pixel resolutions. Those pavement images include a total of 462 crack and non-crack regions containing 128 alligator, 107 longitudinal, 78 transverse cracks and 149 non-crack regions. The connected components were extracted using crack candidate detection algorithm, as explained in Chapter 2.

96 connected components, representing the features of each crack type, were allocated for training of SVMs. In order to prevent the use of unbalanced data for training, the data set consists of equally distributed crack types, i.e., 24 connected regions of each transverse, longitudinal, alligator cracks and non-cracks. The rest of the dataset were used for testing purposes. The details of crack candidate detection and crack classifications are given in the following sections.

4.1. Crack Candidate Detection

Crack and non-crack regions were extracted from the background images using classical image processing techniques. Figure 33 provides the results of these image

processing steps. In this figure, randomly selected images are illustrated for each crack type. Figure 33a shows the input images taken by UAV. All images were resized to 512 x 512 pixels to speed up processing time of the algorithm. They were corrected against non-uniform illumination using morphological operation with a disk-shaped filter. After that wavelet denoising was applied, the results of which is shown in Figure 33b.

The images were then processed using segmentation with an automatically chosen threshold, as shown in Figure 33c. The first (τ_1) and second (τ_2) threshold values are given below the figures, where the final threshold value is given in bold letters. Later, some image enhancements were carried out as the post-processing step (Figure 33d). In this step, median filtering with a rectangle element of 3 x 3 pixels was applied and the regions having the area of maximum 500 pixels were removed. Finally, structures of the crack candidate regions were enhanced using morphological closing operation through diamond shape filter with 5 pixels radius. The final form of crack candidates are shown in Figure 33e.

4.2. Crack Classification

Crack classification was carried out in two stages: (i) SVM training, and (ii) performance testing. For the first part, the geometric features of connected components allocated for SVM training were calculated initially. Then, those features were normalized to [0, 1] range. As a kernel trick, radial basis function kernel (RBF) kernel was selected since (i) the number of instances, i.e., the number of connected regions, were not very big in this study, and (ii) the dimensionality of the transformed space with RBF is infinite. The optimum training parameters of SVM were found using grid search. During grid search, three-fold cross validation was performed for proper

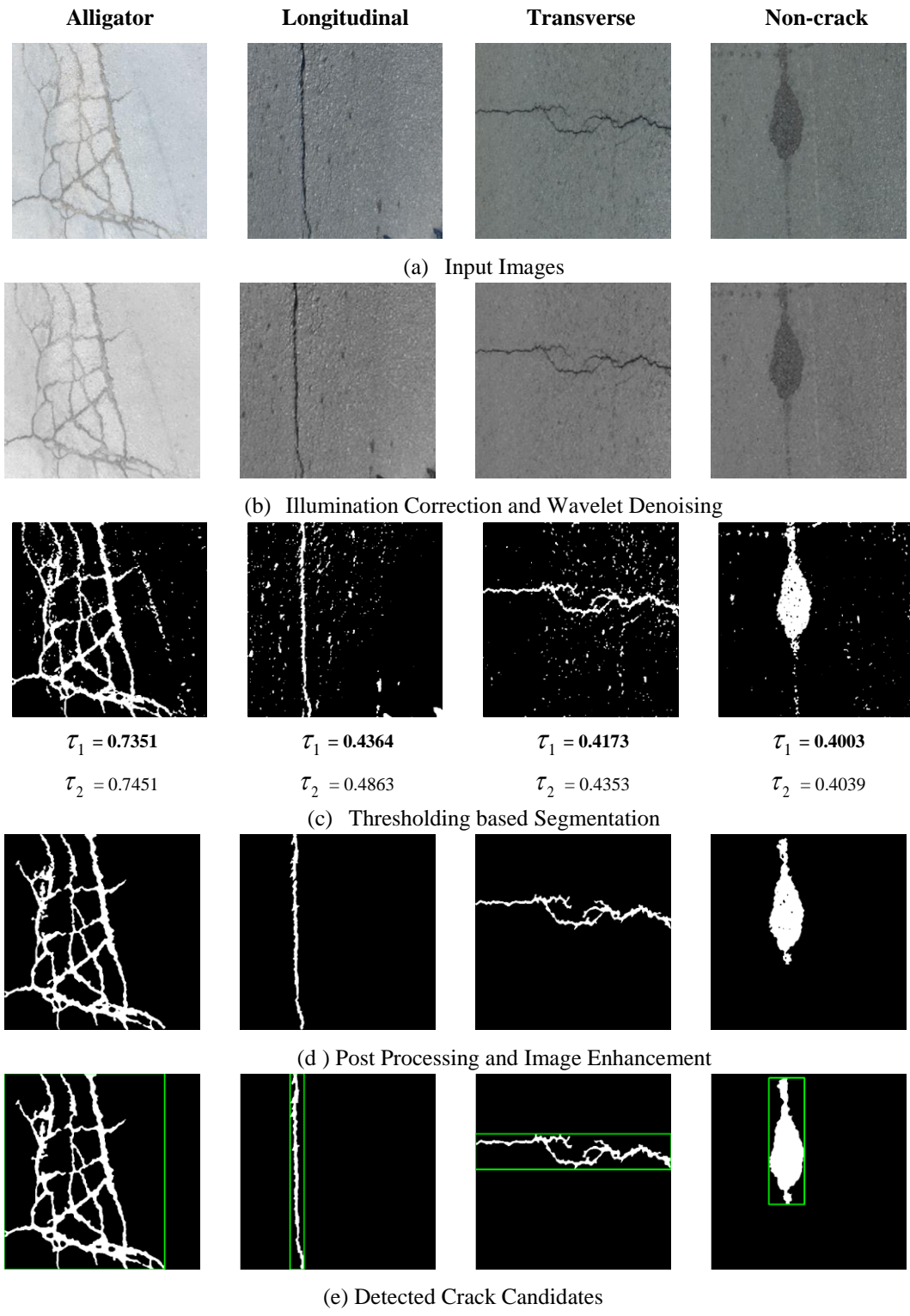


Figure 33 - Results of Crack Candidate Detection Algorithm For Different Crack Categories

learning of the crack types. In three-fold cross validation, first, the training set was divided into 3 subsets equally. To ensure the proper learning, one subset was tested using the classifier trained on the remaining 2 subsets. Hence, each instance of the whole training set was predicted once. The goal was to identify good parameters so that the classifier can predict testing data effectively. After learning parameters were determined, SVM was trained with one against all approach using MATLAB LIBSVM library (Chang & Lin 2011). A sample of training data set is shown in Table 3 where the numbers in the “Output” column correspond to transverse (1), longitudinal (2), alligator (3), non-crack (4) crack types.

Table 3 - Representative Training Data Set

ε	θ	E	R_c	F	S	AR	l	Output
0.9833	0.1218	0.1100	0.0176	0.0657	0.5000	3.9293	1	1
0.9979	0.9974	0.1914	0.0220	0.2055	0.7044	0.0920	-1	2
0.8622	0.6588	0.2858	0.0084	0.2160	0.8632	0.5695	0	3
0.8920	0.5228	0.6922	0.5863	0.9905	0.8906	0.5238	0	4
...

Table 4 - Number of Classified Connected Components

		CRACK CLASSIFICATION			
		Alligator	Longitudinal	Non-crack	Transverse
ACTUAL CRACK TYPE	Alligator	48	14	17	25
	Longitudinal	0	80	3	0
	Non-crack	1	11	111	2
	Transverse	1	0	2	51

In the second part, connected regions that were not used during training were tested using obtained SVM model. The classification results were tabulated in Table 4. In this table, the number “48” in the third row means that total number of 48 crack candidate regions were correctly classified, i.e. they were actually alligator crack and classified as alligator crack. On the other hand, “14” represents that total number of 14

alligator crack regions that were misclassified as longitudinal cracks. Figure 4 presents the classification results using pie charts.

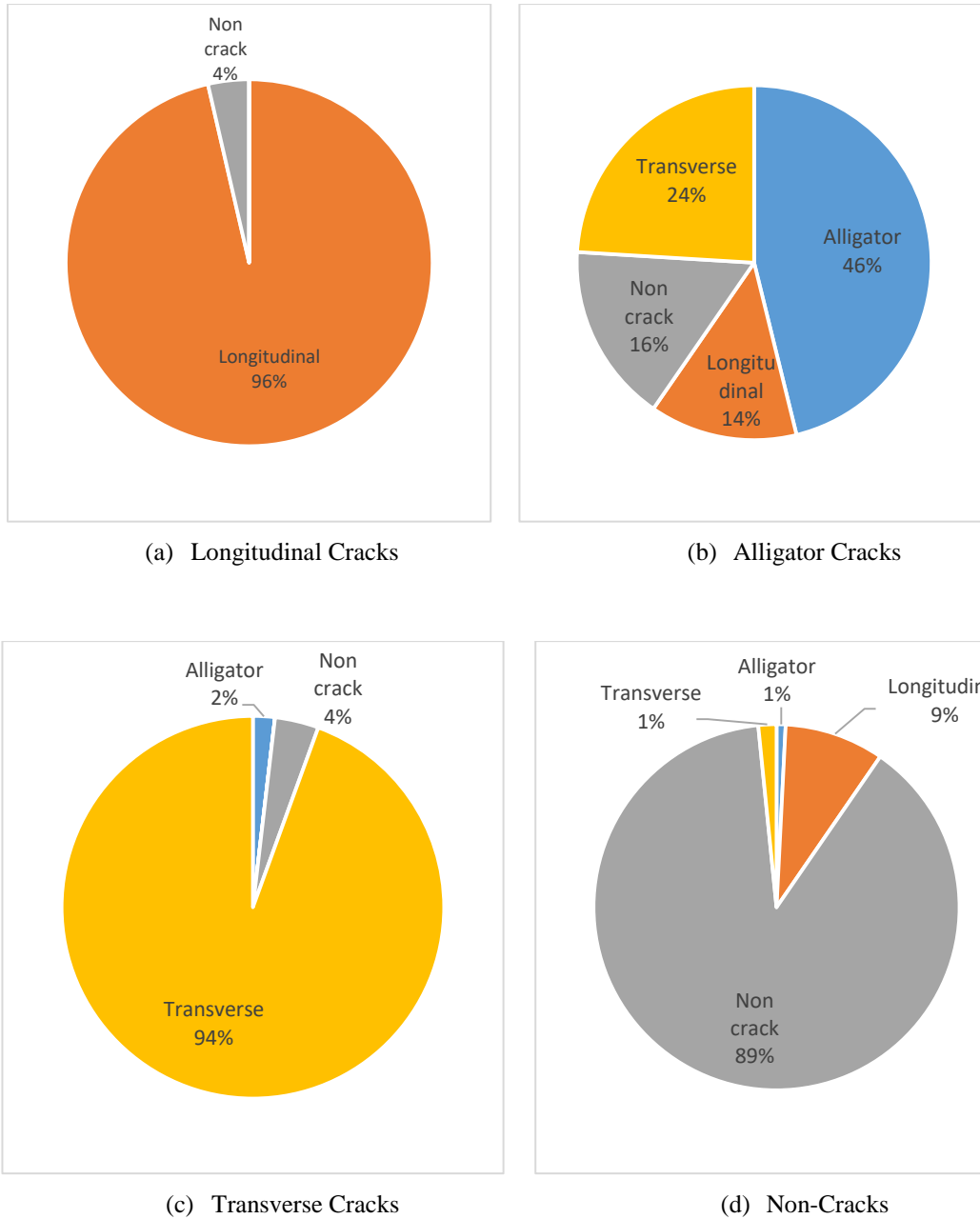


Figure 34 - Classification of Crack Types

4.3. Results and Discussion

The performance of proposed pavement crack identification algorithm is illustrated above. According to the classification results, it was observed that the proposed algorithm has superior ability in classifying the longitudinal crack, transverse crack and non-crack regions. 96% of longitudinal crack regions were successfully detected and classified as their own type (Figure 34a). Although there were some misclassified regions, classification performances for these three type of crack regions are acceptable. These misclassified regions generally occurred when one of the crack regions mimics the other crack types and non-crack regions. As shown in Figure 35, some non-crack regions led to misclassification as they are very thin and resemble longitudinal cracks.

Even though, longitudinal/transverse crack and non-crack regions were classified with a high successful rate, the algorithm have some weaknesses when classifying alligator crack regions. The low percentage of classification performance, 46%, is because of the alligator cracks' complex shape. Unfortunately, more than half of alligator crack regions were classified as other cracks rather than the alligator ones. Since alligator cracks are thinner compared to other types, it is very difficult to maintain their connectivity within their crack shapes. When an optimum thresholding was applied to extract its full body from the background image, some parts of alligator cracks were broken apart from their main body. The broken parts could be classified as longitudinal/transverse cracks or sometimes non-crack regions. As shown in Figure 36, two connected regions were detected, both of which actually belonged to the same alligator crack. However, broken part of alligator crack was classified as longitudinal crack due to its geometric properties.

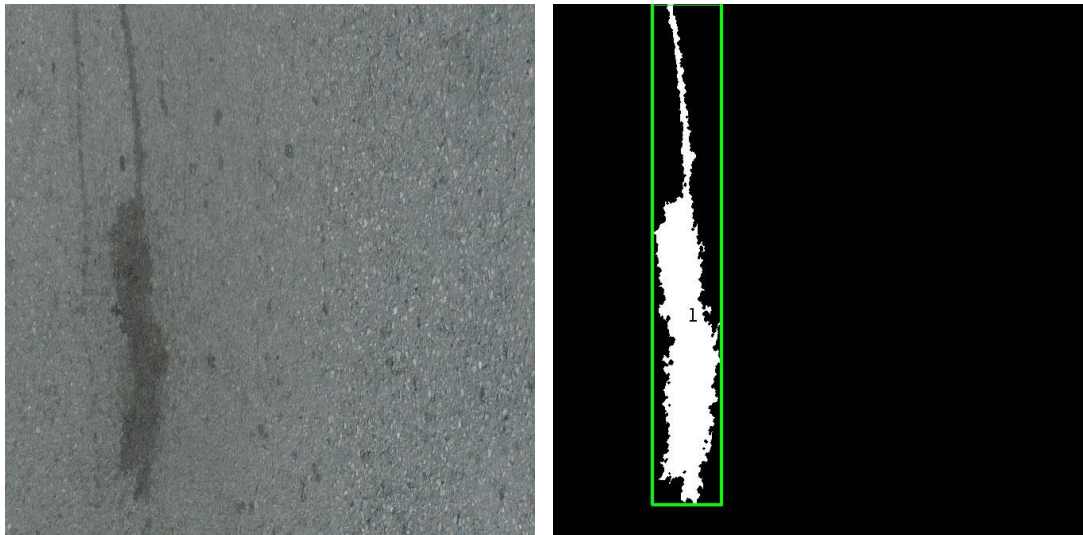


Figure 35 - Actually Non-Crack Region Classified As Longitudinal Crack

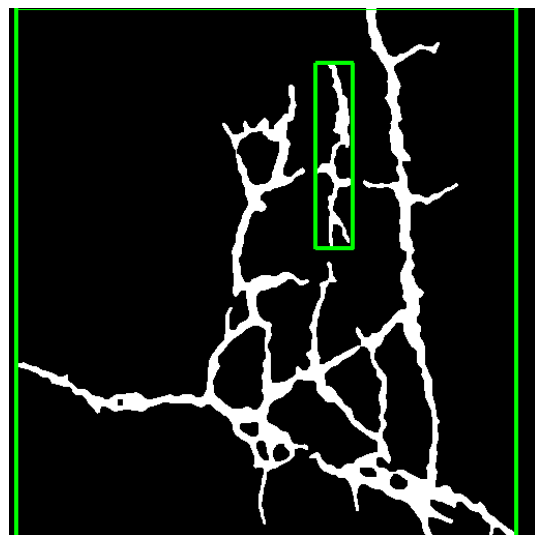


Figure 36 - Broken Alligator Crack

The overall performance of the method is calculated by two different success measures: (i) accuracy of crack detection and (ii) accuracy of crack classification. The accuracy of crack detection can be calculated as the sum of correctly detected crack and non-crack regions divided by the total number of classifications. On the other

hand, the accuracy of crack classification can be calculated as the ratio of the total number of correct classifications of crack types to the total number of classifications. Recall, precision, specificity measures of each crack type are also calculated and tabulated in Table 5.

$$Acc.\text{ of Cr. Det.} = \frac{48+14+25+80+111+1+51}{48+14+17+25+80+3+1+11+111+2+1+2+51} = 90.16\%$$

$$Acc.\text{ of Cr. Class.} = \frac{48+80+111+51}{48+14+17+25+80+3+1+11+111+2+1+2+51} = 79.23\%$$

Table 5 - Statistical Measures

	Alligator	Longitudinal	Non-crack	Transverse
Precision	0.96	0.76	0.83	0.65
Recall/Sensitivity	0.48	0.96	0.89	0.94
Specificity	0.99	0.91	0.91	0.91

The accuracy of crack detection 90.16% shows that the algorithm works effectively to differentiate crack regions from the non-crack ones. In other words, the algorithm classifies crack regions as cracks correctly, which makes the method practically applicable for crack detection purposes. The 79.23% accuracy of crack classification is less than the accuracy of crack detection because of the existence of misclassified alligator crack regions as discussed above.

It should be kept in mind that; the resolution of images was limited due to the camera which was built into UAV through its manufacturers, which also decreases the accuracy of crack classification. Therefore, the proposed system is capable of detecting cracks on the pavements surface which are as small as 6 mm as measured through manual surveys.

The literature surveys indicate that, this may be the first study that proposes UAV together with the connected component based crack identification algorithm. For this reason, it may not be appropriate to make direct comparison with other studies based on the accuracy of the results. Therefore, these comparisons are omitted. However, the advantages and disadvantages of the proposed method can still be compared with current pavement crack identification methods, which are summarized below:

Since most of the crack candidate regions can be distinguished during the binarization step of the algorithm, the proposed UAV based system has considerably fast run-times. The algorithm can successfully segment crack candidate regions and classify them roughly in 2 seconds in a personal computer with an Intel Core i7-3770 CPU 3.40 GHz processor, 16 GB RAM, running on Windows 10 operating system. This is mainly because of the SVM's reusability. Once trained with enough representative crack candidates, the SVM model can be used anytime without the need of acquiring extra images for training. Moreover, since the SVM model works on the features of the connected components instead of images, the method can be used to classify multiple cracks in a single image as demonstrated in Figure 37. This ability can be exploited in the future considering that a UAV can fly high enough to capture multiple lanes at once.

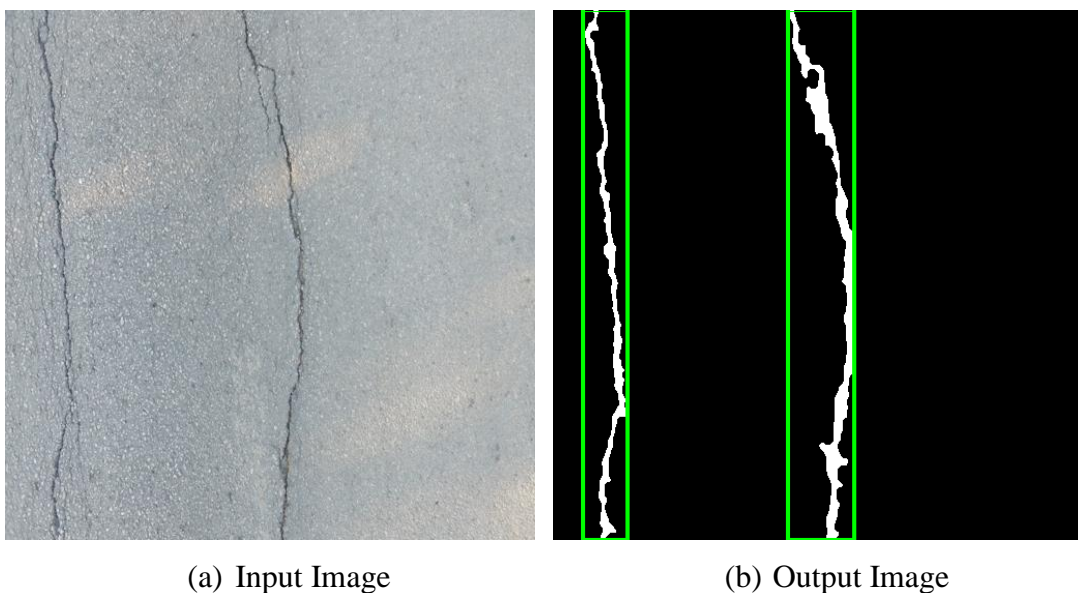


Figure 37 - Multiple Crack Identification

The UAV used in this study, offers economic and better flexibility compared to traditional platforms. In contrast to truck mounted camera based road monitoring systems, it is cheap and easily transportable. Manual methods and truck-based methods may cause traffic disruption due to traveling in a slow speed. However, that remote-controlled UAV can fly over a certain height, so it does not interrupt vehicles, which makes the system a good practical solution even under heavy traffic (Koch et al. 2015). Also, with the latest software update of model used in this study, pre-planning and autonomous flight over a pavement are possible. Therefore, longer roads can be scanned for cracks in a very quick and secure way now.

In spite of the advantages of the UAV aided algorithm, the system has some challenges to overcome to be more effective. First, like many image based crack identification algorithms, illumination is a serious concern. Since proposed UAV system does not have its own illumination resource, it is not possible to work at the night time. The experiments should be done during day time. Moreover, the weather conditions also affect the performance of the UAV as well as the quality of the acquired images. The stability of device becomes unreliable when the wind speed is above a certain threshold, which is generally provided by the manufacturer. Since the device has electric powered motors, it is not safe to fly in rainy or snowy weather conditions.

Considering the most UAV devices rely on GPS services for navigation, in the areas where the GPS coverage is poor, there will be inaccuracies in UAV's control system. This might hinder the devices ability to keep flying at fixed altitudes, which leads to taking pictures from changing distances. Moreover, when UAVs with no automatic collision avoidance system are used, there may be collisions with obstacles along the road such as tree branches or road signs.

During the experiments, the maximum altitude was selected as 3 meters. This is because the UAV does not have a camera with optical zoom feature. Therefore, at altitudes above 3 meters, the crack candidate regions in the images are very small and thus detection algorithm cannot work efficiently. An alternative solution to eliminate this problem would be using an octocopter/hexacopter UAV with a DSLR camera

payload or utilizing a camera with larger sensor size. This way, the UAV can fly high enough such that the traffic underneath is not disrupted and high resolution images can be collected.

CHAPTER 5

SUMMARY, CONCLUSIONS AND FUTURE WORK

5.1. Summary

Together with the increase in daily traffic operations and heavy weight transportation activities, structural condition of pavements gets worse and needs to be monitored at more regular intervals. In order to apply effective rehabilitation and maintenance strategies on pavements, the cracks on the pavement surfaces need to be correctly identified. These assessments assist transportation agencies to estimate the future conditions in terms of supporting an investment plan for reconstruction or allocating maintenance and repair resources. In order to evaluate the current condition of existing pavements in a proper way, the use of a functional and cost effective Pavement Management System is compulsory.

The old fashioned methods for monitoring pavements are the use of manual inspections, in which the experts are walking on the roads and making visual inspections. To overcome the easily foreseen disadvantages, with the development of modern tools and algorithms, automated pavement monitoring and inspection systems have gained more attention to meet the increasing demands to have intelligent pavement management platforms. Automated pavement inspection systems can be categorized into two parts as data collection and data processing. In data collection part, pavement surface information is gathered as 2D images or 3D surface data by using moving vehicles. Whatever the data collection tool is, the collected data need to

be processed using image processing and sophisticated learning algorithms. In this sense, computer vision methods and machine learning become an essential component of modern Structural Health Monitoring systems.

In this study, the main focus was to develop a robust pavement crack identification system, in which a powerful crack identification algorithm we developed was applied to images taken by UAV from the surface of pavements in order to identify the cracks and classify them successfully. The proposed pavement crack identification method consists of two stages: (i) crack candidate detection, (ii) crack classification. In the crack candidate detection part, potential crack regions are extracted using some image enhancement and segmentation techniques. A background subtraction algorithm is applied to ensure the same background lighting condition for all pavement images. Then, wavelet based image denoising is implemented to remove the noise in the signal. For the purpose of segmenting crack regions, a self-adaptive local thresholding method is utilized and a binary image is obtained. As a last step, crack candidate regions are purified from the noises by using median filtering and morphological closing operation. Once crack candidate regions are obtained, it is aimed to classify the candidates into four different types: longitudinal, transverse, alligator and non-crack. To do that, a supervised machine learning algorithm Support Vector Machine (SVM) is properly trained using varied geometric properties of candidate regions which are labeled by field experts. Finally, the rest of crack candidate regions are classified by using the developed SVM model.

For the purpose of testing proposed pavement crack identification system, several experiments were performed along the roads of Middle East Technical University campus. Pavement photos including crack and non-crack regions were collected during daylight conditions. With the camera of a quadcopter called DJI Inspire 1, a total of 261 pavement photos were taken facing directly towards the pavement and stored to its micro SD card. Then, collected photos were transferred to computer in order to process them offline. Total of 462 regions were obtained using crack candidate detection algorithm.

A part of data set, which well represents the features of crack type, were allocated for SVM training and rest of them were left for performance evaluation of the proposed pavement crack identification algorithm. After the SVM model was obtained successfully, remaining candidate regions were tested using that model.

5.2. Conclusions

In this study, we present a novel pavement crack identification system using UAVs, which are employed as data collection tools from the surface of pavements. The proposed system has an image processing analysis and classification engine that is developed using ordered combinations of classical image processing techniques and a powerful classifier called SVM. The proposed system can be used for determining and classifying the three most commonly encountered crack types: (i) longitudinal, (ii) transverse, and (iii) alligator cracks. In addition, it can detect non-cracks on the pavement surface to prevent obtaining false positive results.

The classification results showed that the proposed algorithm has superior ability in classification of longitudinal crack, transverse crack and non-crack regions. There were few misclassification regions since some crack and non-crack regions resembled each other. The performance of classification alligator crack was not successful as other crack types. Because of alligator cracks' complex and varying shapes, some alligator cracks were classified as longitudinal cracks, transverse cracks and non-cracks. The main factor behind these misclassifications were the disjointed parts of alligator crack from its main body. Considering all of these details, the total accuracy of the pavement crack detection and crack classification was computed as 90.2%, 79.2%, respectively. This was a quite reasonable performance for a UAV based pavement crack identification system to be used in practical applications effectively.

The originality of this study lies in the fact that UAVs are used for the first time together with the connected component based crack identification algorithm for

pavement crack detection and classification. UAV platforms comprise economic and easy to use solutions compared to truck-based methods. With the advancements of their technology, robustness and the reliability of the devices improves, which makes UAVs a more trustworthy way for monitoring applications. Since the devices used for monitoring applications do not weigh more than 5 kilograms, this makes the system considerably mobile. Beside their mobility, UAVs do not cause traffic disruption. They can fly over a certain height in order not to interrupt vehicles even under heavy traffic. This is a unique advantage and a good practical solution for pavement condition monitoring.

The heart of the proposed pavement crack identification algorithm is formed by connected components based identification. Since geometric properties of cracks obtained from the connected regions instead of pixels, both training and testing data are reduced considerably. Using connected component not only decrease computational cost but also it provides the capability of multiple crack and non-crack identification in one single image.

Despite the advantages of the UAV based method, the system still has some challenges to overcome to be more effective. First, like in many image based crack identification algorithms, illumination is a serious concern. Depending on which time of the day the experiments are performed, image quality changes significantly. Although, a background illumination correction algorithm is implemented to get rid of the improper illumination, if the light coming from the sun is not sufficient, the success rate of crack candidate detection decreases noticeably. Having an illumination system mounted on a UAV may solve that problem and also gives an ability to work at night time. The image quality and the performance of the UAV is also affected by weather conditions. When the wind speed is above its operation limit, the device becomes unstable and it is not safe to make a measurement in such conditions. Rainy and snowy weather conditions also have an effect on the decision whether to fly the UAV or not.

5.3. Future Work

The proposed system is under continuous development to work reliably for a fully automated pavement crack identification system. The following recommendations are highlighted to be studied in the future:

- Pavement crack identification engine should be integrated with image acquisition tool. SVM training should be performed in a powerful computer offline, but the obtained SVM model and crack detection algorithm needs to be embedded into electronic card of the UAV. By doing this, a real time pavement crack identification can be developed.
- With the latest update of UAV control software, flight missions can be planned before operating the UAV. This way autonomous pavement monitoring can be carried out regularly using the pre-determined missions.
- In this study, the maximum altitude was selected as 3 meters in the experiments. The main reason of this selection is that the employed UAV does not have a camera with optical zoom feature. Therefore, the crack detection algorithm cannot work efficiently above 3 meters, because crack regions are small and thin. As an alternative, UAV with high resolution DSLR camera payload can be used to handle the resolution problem. This way, the UAV can fly high enough such that it does not affect the traffic underneath it.
- Using crack regions as connected components gives a flexibility to define different kind of crack types. Therefore, new types of cracks can be outlined in the model using distinctive geometric properties. Moreover, non-crack regions including tire marks, oil stains and shadows of UAVs can also be separated from each other.
- Since all images taken by UAV have GPS coordinates in their documented file properties, locations of cracks are actually known. A GIS integration can be developed to read image coordinates automatically and place them in a map using their latitude and longitude coordinates. This map may give valuable information for state highway agencies and local authorities.

- The proposed crack identification system was applied for the surface cracks on flexible pavements. However, since the crack segmentation algorithm is automated, the settings of algorithm are adjusted automatically, type of the pavement can easily be changed to concrete pavements. To properly test the performance of the proposed system on concrete pavement, an experimental study is planned in the very near future.

REFERENCES

- Awad, M. & Khanna, R., 2015. *Efficient Learning Machines* 1st Ed., New York: Apress Media.
- Bendea, H. et al., 2008. Low Cost UAV for Post-Disaster Assessment. *Proceedings of The XXI Congress of the International Society for Photogrammetry and Remote Sensing Beijing China 311 July 2008*, XXXVII, pp.1373–1380.
- Boser, B.E., Guyon, I.M. & Vapnik, V.N., 1992. A Training Algorithm for Optimal Margin Classifiers. *Proceedings of the Fifth Annual ACM Workshop on Computational Learning Theory*, pp.144–152.
- Chang, C. & Lin, C., 2011. LIBSVM : A Library for Support Vector Machines. *ACM Transactions on Intelligent Systems and Technology (TIST)*, 2, pp.1–39.
- DJI, 2016. DJI Inspire 1 Specifications. *DJI*. Available at: <http://www.dji.com/product/inspire-1/info> [Accessed August 30, 2016].
- Ellenberg, A. et al., 2014. Masonry Crack Detection Application of Unmanned Aerial Vehicle. *The Sixth International Conference on Computing in Civil and Building Engineering*, pp.1179–1184.
- Eschmann, C. et al., 2013. High-Resolution Multisensor Infrastructure Inspection With Unmanned Aircraft Systems. *International Archives of the Photogrammetry, Remote Sensing and Spatial Information Sciences*, XL(September), pp.4–6.
- Eschmann, C., Kuo, C. & Boller, C., 2012. Unmanned Aircraft Systems for Remote Building Inspection and Monitoring. *Proceedings of the 6th European Workshop on Structural Health Monitoring, July 3-6, 2012, Dresden, Germany*, pp.1–8.
- Feng, W., Yundong, W. & Qiang, Z., 2009. UAV Borne Real-Time Road Mapping System. *2009 Joint Urban Remote Sensing Event*, pp.1–7.
- Fresques, L., 2009. Student Engineers Assist NMDOT with Highway Condition Assessments. *New Mexico State University*. Available at: <https://newscenter.nmsu.edu/articles/view/4780> [Accessed August 30, 2016].
- Fukuhara, T. et al., 1990. Automatic Pavement-Distress-Survey System. *Journal of Transportation Engineering*, 116(3), pp.280–286.

- Gavilán, M. et al., 2011. Adaptive Road Crack Detection System By Pavement Classification. *Sensors*, 11(10), pp.9628–9657.
- Gonzalez, R.C. & Woods, R.E., 2008. *Digital Image Processing* Third Edit., Pearson, Prentice Hall.
- Groeger, J.L. et al., 2003. Implementation of Automated Network Level Crack Detection Processes in the State of Maryland. *Annual Meeting of Transportation Research Board*, (410).
- Gungor, O.E. & Pekcan, O., 2013. Connected Component Based Pavement Crack Identification Using Support Vector Machines. In *Proceeding of the TRB Annual Meeting 2013*.
- Huang, Y. & Xu, B., 2006. Automatic Inspection of Pavement Cracking Distress. *Journal of Electronic Imaging*, 15(1), p.13017.
- Kenneth, H.M., 2004. NCHRP Synthesis 334: Automated Pavement Distress Collection Techniques. *Transportation Research Board, National Research Council, Washington, D.C.*, 334.
- Klassen, G. & Swindall, B., 1993. Automated Crack Detection System Implementation in ARAN. In *Digital Image Processing: Techniques and Applications in Civil Engineering*. p. 9.
- Koch, C. et al., 2015. A Review on Computer Vision Based Defect Detection and Condition Assessment of Concrete and Asphalt Civil Infrastructure. *Advanced Engineering Informatics*, 29(2), pp.196–210.
- Li, Q. et al., 2011. FoSA: F* Seed-growing Approach for Crack-line Detection From Pavement Images. *Image and Vision Computing*, 29(12), pp.861–872.
- Mallat, S.G., 1989. A Theory for Multiresolution Signal Decomposition: The Wavelet Representation. *IEEE Transactions on Pattern Analysis and Machine Intelligence*, II(7).
- Mathworks, 2016. Morphological Structuring Element. Available at: <http://www.mathworks.com/help/images/ref/strel-class.html> [Accessed August 28, 2016].
- Miller, J.S. & Bellinger, W.Y., 2003. *Distress identification manual for the long-term pavement performance program*. Federal Highway Administration Report,
- Nguyen, T.S., Avila, M. & Begot, S., 2009. Automatic Detection and Classification of Defect on road Pavement using Anisotropy Measure. *European Signal Processing Conference*, (Eusipco), pp.617–621.

- Oliveira, H. & Correia, P.L., 2013. Automatic Road Crack Detection and Characterization. *IEEE Transactions on Intelligent Transportation Systems*, 14(1), pp.155–168.
- Oliveira, H. & Correia, P.L., 2009. Automatic Road Crack Segmentation Using Entropy and Image Dynamic Thresholding. *European Signal Processing Conference*, (Eusipco), pp.622–626.
- Otsu, N., 1979. A Threshold Selection Method from Gray-level Histograms. *IEEE Transactions on Systems, Man, and Cybernetics*, 9(1), pp.62–66.
- Rangarajan, R., Venkataraman, R. & Shah, S., 2002. Image Denoising Using Wavelets.
- Richards, J.A., 2013. *Remote Sensing Digital Image Analysis* Fifth Edit., New York.
- Salari, E. & Bao, G., 2010. Pavement Distress Detection and Classification Using Feature Mapping. *2010 IEEE International Conference on Electro/Information Technology, EIT2010*.
- Salvatore Cafiso, A.D.G. & Battiato, S., 2006. Evaluation of Pavement Surface Distress Using Digital Image Collection and Analysis. *Seventh International Congress on Advances in Civil Engineering. Istanbul, Turkey*, pp.1–10.
- Schnebele, E. et al., 2015. Review of Remote Sensing Methodologies for Pavement Management and Assessment. *European Transport Research Review*, 7(2).
- Sy, N.T. et al., 2008. Detection of Defects in Road Surface by a Vision System. *Proceedings of the Mediterranean Electrotechnical Conference - MELECON*, 2(c), pp.847–851.
- T.C. Maliye Bakanlığı Bütçe ve Mali Kontrol Genel Müdürlüğü, 2016. 2016 Yılı Merkezi Yönetim Bütçe Kanunu. Available at: <http://www.bumko.gov.tr/TR,61/butce-kanunu-ve-ekleri.html> [Accessed August 30, 2016].
- Tatham, P., 2009. An Investigation Into the Suitability of the Use of Unmanned Aerial Vehicle Systems (UAVS) the Initial Needs Assessment Process in Rapid Onset Humanitarian Disasters. *International Journal of Risk Assessment and Management*, 13(1), pp.60–78.
- Tsai, Y. et al., 2015. Innovative Crack Sealing Analysis and Cost Estimation for Airport Runway Shoulders Using 3D Laser Technology and Automatic Crack Detection Algorithms. *Airfield and Highway Pavements 2015*, pp.652–661.

- Tsai, Y.-C.J. & Li, F., 2012. Critical Assessment of Detecting Asphalt Pavement Cracks under Different Lighting and Low Intensity Contrast Conditions Using Emerging 3D Laser Technology. *Journal of Transportation Engineering*, 138(5), pp.649–656.
- U.S. Department of Transportation, 2016. Budget Highlights Fiscal Year 2016. Available at: <https://www.transportation.gov/mission/budget/fiscal-year-2016-budget-highlights> [Accessed August 30, 2016].
- Wang, K.C.. et al., 2002. Data Analysis of Real-Time System for Automated Distress Survey. *Transportation Research Record*, 1806(2), pp.101–109.
- Wang, K.C.. & Elliot, R.P., 1999. *Investigation of Image Archiving for Pavement Surface Distress Survey, A Final Report*,
- Wang, K.C.P. et al., 2003. Network Level Crack Survey with the Automated Real-Time Distress Analyzer. *Annual Meeting of Transportation Research BoardTransportation Research Board*, pp.1–26.
- Zhang, C., 2008. An UAV-based Photogrammetric Mmapping System for Road Condition Assessment. In *The International Archives of the Photogrammetry, Remote Sensing and Spatial Information Sciences*. pp. 627–632.
- Zhang, C. & Elaksher, A., 2011. An Unmanned Aerial Vehicle-Based Imaging System for 3D Measurement of Unpaved Road Surface Distresses. *Computer-Aided Civil and Infrastructure Engineering*.
- Zhao, H., Qin, G. & Wang, X., 2010. Improvement of Canny Algorithm Based on Pavement Edge Detection. *Proceedings - 2010 3rd International Congress on Image and Signal Processing, CISPA 2010*, 2, pp.964–967.
- Zhou, J., S. Huang, P. & Chiang, F.-P., 2006. Wavelet-based Pavement Distress Detection and Evaluation. *Optical Engineering*, 45(2), p.27007.
- Zou, Q. et al., 2012. CrackTree: Automatic Crack Detection From Pavement Images. *Pattern Recognition Letters*, 33(3), pp.227–238.